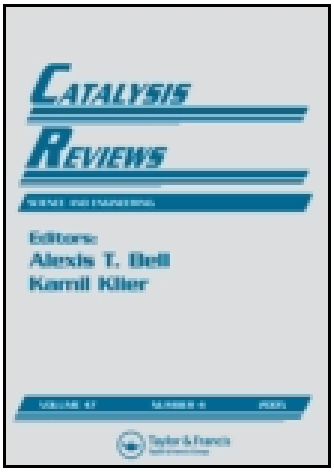

Catalysis Reviews: Science and Engineering

Publication details, including instructions for authors and subscription information:
http://www.tandfonline.com/loi/lctr20

A Review on the Pd-Based Three-Way Catalyst

Jihui Wang[a], Hong Chen[ab], Zhicheng Hu[c], Mingfa Yao[b] & Yongdan Li[ab]

[a] Collaborative Innovation Center of Chemical Science and Engineering (Tianjin), Tianjin Key Laboratory of Applied Catalysis Science and Technology, State Key Laboratory of Chemical Engineering (Tianjin University), School of Chemical Engineering, Tianjin University, Tianjin, China

[b] State Key Laboratory for Engines, School of Mechanical Engineering, Tianjin University, Tianjin, China

[c] Weifu Environmental Catalysts Co. Ltd, Wuxi, Jiangsu, China

Published online: 25 Nov 2014.

To cite this article: Jihui Wang, Hong Chen, Zhicheng Hu, Mingfa Yao & Yongdan Li (2015) A Review on the Pd-Based Three-Way Catalyst, Catalysis Reviews: Science and Engineering, 57:1, 79-144, DOI: 10.1080/01614940.2014.977059

To link to this article: http://dx.doi.org/10.1080/01614940.2014.977059

Catalysis Reviews: Science and Engineering, 57:79–144, 2015

ISSN: 0161-4940 print / 1520-5703 online
DOI: 10.1080/01614940.2014.977059

Taylor & Francis
Taylor & Francis Group

A Review on the Pd-Based Three-Way Catalyst

Jihui Wang[1], Hong Chen[1,2], Zhicheng Hu[3], Mingfa Yao[2], and Yongdan Li[1,2]

[1]Collaborative Innovation Center of Chemical Science and Engineering (Tianjin), Tianjin Key Laboratory of Applied Catalysis Science and Technology, State Key Laboratory of Chemical Engineering (Tianjin University), School of Chemical Engineering, Tianjin University, Tianjin, China
[2]State Key Laboratory for Engines, School of Mechanical Engineering, Tianjin University, Tianjin, China
[3]Weifu Environmental Catalysts Co. Ltd, Wuxi, Jiangsu, China

The application of Pd in three-way catalyst represents a significant technology breakthrough for the removal of pollutants from gasoline powered vehicle exhaust gas. Pd shows superior catalytic activity for hydrocarbon (HCs) oxidation and thermal stability to the conventional Pt/Rh catalyst. However, Pd catalysts are more susceptible to chemical poisoning. This work summarizes the progress of the Pd-based three-way catalyst and its related technologies. The state of Pd in the reaction, the support and oxygen storage material, the promoters, and preparation methods on the catalytic performance are reviewed. The process and catalyst configurations, e.g., close-couple (CCC), dual bricks, layered, and zone-coated catalysts, are described and compared. The advances in the understanding of the reaction and deactivation mechanisms in the three-way catalysis systems are also discussed.

Keywords Three-way catalyst, Oxygen storage capacity, Palladium, Catalyst configuration, Mechanism and kinetics

1. INTRODUCTION

Serious concerns in urban air quality deterioration caused by automotive emissions and the more harmful species evolved from them via photochemical reactions, were noticed as early as the 1970s due to the increased use of vehicles (1). In American cities such as Los Angeles, photochemical smog occurred

Received 1 January 2014; accepted 23 September 2014.

Address correspondence to Yongdan Li, Collaborative Innovation Center of Chemical Science and Engineering (Tianjin), Tianjin Key Laboratory of Applied Catalysis Science and Technology, State Key Laboratory of Chemical Engineering (Tianjin University), School of Chemical Engineering, Tianjin University, Tianjin 300072, China. E-mail: ydli@tju.edu.cn

so frequently that air quality became a major health problem at the time. The origin of the photochemical smog can be ascribed to the reaction occurring between two of the primary pollutants (unburned hydrocarbons and nitrogen oxides) of automotive emissions with the promotion of sunlight:

$$\mathrm{HC} + \mathrm{NO}x + \mathrm{hv} \rightarrow \mathrm{O_3} + \text{other products.} \tag{1}$$

Typical exhaust gas composition of the gasoline engine powered vehicles at the normal operating conditions is carbon monoxide (CO, 0.5 vol.%), unburned hydrocarbons (HC, 350 ppmv), nitrogen oxides (NOx, 900 ppmv), hydrogen (H_2, 0.17 vol.%), water (H_2O, 10 vol.%), carbon dioxide (CO_2, 10 vol.%), oxygen (O_2, 0.5 vol.%), and nitrogen left (2). Among these species, HC, CO, and NOx are the major harmful pollutants. Catalysts for the treatment of automotive exhaust gas have been developed since 1974 when these catalysts were commercialized in the U.S. and Japan (3). Now, the catalysts are widely applied for the control and suppression of the environmental impact of the exhaust emission of the gasoline-powered vehicles by converting the basic air contaminants CO, HCs, and NOx to their corresponding harmless products CO_2, N_2, and H_2O (4). This concept was christened as the three-way catalyst (TWC) (5). The main reactions in this catalysis system can be described with Eqs. (2)–(9) (2,6)
Oxidation reactions:

$$\mathrm{C_mH_n} + \mathrm{O_2} \rightarrow \mathrm{CO_2}\,(\mathrm{CO}) + \mathrm{H_2O} \tag{2}$$

$$\mathrm{CO} + \mathrm{O_2} \rightarrow \mathrm{CO_2} \tag{3}$$

$$\mathrm{H_2} + \mathrm{O_2} \rightarrow \mathrm{H_2O} \tag{4}$$

NO Reduction reactions:

$$\mathrm{C_mH_n} + \mathrm{NO} \rightarrow \mathrm{N_2}\,(\mathrm{N_2O}, \mathrm{NH_3}) + \mathrm{H_2O} + \mathrm{CO_2} \tag{5}$$

$$\mathrm{CO} + \mathrm{NO} \rightarrow \mathrm{CO_2} + \mathrm{N_2}(\mathrm{N_2O}) \tag{6}$$

$$\mathrm{H_2} + \mathrm{NO} \rightarrow \mathrm{N_2}\,(\mathrm{N_2O}, \mathrm{NH_3}) + \mathrm{H_2O} \tag{7}$$

Hydrogen production reactions:

$$\mathrm{CO} + \mathrm{H_2O} \rightarrow \mathrm{CO_2} + \mathrm{H_2} \tag{8}$$

$$\mathrm{C_mH_n} + \mathrm{H_2O} \rightarrow \mathrm{CO_2} + \mathrm{H_2} \tag{9}$$

The TWCs typically consist of (1) a cordierite or stainless steel-based monolithic substrate having a honeycomb structure, (2) high surface area support and oxygen storage materials coated on the monolith, (3) the platinum group metals (Pt, Pd, and Rh) which act as the active components, and (4) metal oxides that are mainly functioned as the promoters (7,8). Advances in monolith technology and catalyst-mounting methods, flexibility in reactor design, low pressure drop, high heat and mass transfer rates, are the main reasons for adopting monolithic substrates (2). The ceramic substrates are often based on cordierite ($2MgO{\cdot}2Al_2O_3{\cdot}5SiO_2$) material. γ-Al_2O_3 was used as the major component of the first coating layer or the basic catalyst support on the monolithic cordierite, due to its high surface area and relatively good thermal stability under the hydrothermal conditions of the exhaust gas (9). At air fuel ratios close to the stoichiometric point, the TWCs work efficiently and achieve a simultaneous conversion of CO/HCs/NOx. A typical response of the TWC as a function of the air/fuel ratio is shown in Fig. 1. As reported by Gandhi et al. (5), the addition of CeO_2 to the basic support of the TWCs enhances CO, HC, and NOx conversions under the conditions with lean-rich swings of the exhaust gas composition. When the fuel is rich, oxygen content is insufficient for the complete oxidation of CO and HC. In the lean mode, oxygen in the exhaust is too high, which leads to a low NOx reduction conversion. Ceria in the catalyst adsorbs and releases oxygen in response to the oxygen/fuel ratio in the exhaust gas, due to the Ce^{4+}/Ce^{3+} redox reactions. The capability of the catalyst in storing and releasing oxygen became an important factor. In general, this capacity is classified as oxygen storage capacity (OSC) and dynamic OSC (DOSC). OSC refers to the amount of oxygen thermodynamically available, while DOSC is related to the amount of oxygen kinetically available during

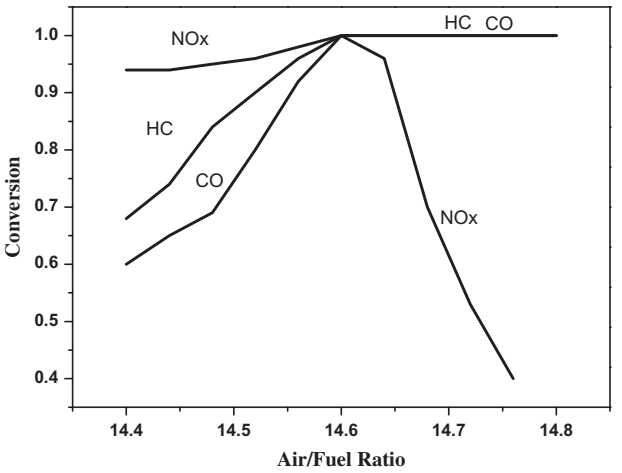

Figure 1: The typical performance of three-way catalyst as a function of the air/fuel ratio.

transient conditions. In addition to the OSC, the introduction of CeO_2 to Pd-TWCs also enhances the activity of water-gas shift (WGS) and steam reforming reactions which favors the removal of the carbon monoxide and hydrocarbons (10,11). As the content of water vapor reaches about 10 vol% in the exhaust gas, the high activity of WGS and steam reforming reactions may remarkably contribute to the three-way reactions. The main limitation for the application of pure CeO_2 is the poor thermal stability because the vehicle exhaust condition is thermally hash. With the reaction temperature higher than 800°C, the catalyst with pure CeO_2 in the support experienced deactivation seriously. Thereafter, the incorporation of ZrO_2 into the CeO_2 lattice has been proved to be effective in preventing CeO_2 from sintering and improving the OSC, leading to a better performance of the TWCs (12–14).

In the early 1970s, Pt and Pt/Pd in various ratios were employed as the active components in the automotive emission control catalysts, which were evolved from the early oxidation catalysts for the complete oxidation of CO and HCs (15–17). Meguerian et al. (18) discovered the necessity of Rh in reducing NO*x*. Afterwards, as stricter NO*x* standards were introduced in the 1980s, Pt was combined with Rh to convert CO, HC, and NO*x* simultaneously (19). NO*x* from the engine exhaust can be efficiently reduced to N_2 with the in stream reducing species like HCs and CO over the Pt/Rh catalyst in fuel rich exhaust gas (20). Furthermore, a Pt/Rh synergistic effect in the Pt-Rh TWCs was found by Hu et al. (21,22). Pt helps to keep Rh in active and dispersed metallic state through H_2 spillover from Pt particles, which facilitates the regeneration of the inert Rh-alumina species formed under oxidizing conditions at high temperatures. Pt/Rh containing catalysts dominated the automobile exhaust converter market for many years. However, the cost of Pt and Rh are both very high especially for Rh, which has been produced in very small quantity in the world (23). Extensive efforts have been paid to find the replacement of the very rare Pt and Rh in automotive catalyst, which has to meet the more and more stringent emission standards. Pd, which is more abundant and adequate in supply, drew much attention to reduce the cost with precious metals. The Pd catalysts developed thereafter demonstrated significantly improved light-off and NO*x* conversion activities compared to the commercial Pt/Rh TWCs (24). Ford introduced a Pd/Rh catalyst in 1989, in which Pt was replaced with Pd (25,26). However, Pd forms alloy with Rh and enriches at the surface, which strongly suppresses the excellent catalytic activity of Rh (27). Furthermore, Pd tends to form PdO on the surface in oxygen rich atmosphere, which further restrict the good performance of Rh (28,29). In 1994, Ford Motors firstly successfully applied the Pd-only TWCs from Engelhard, and met the then most stringent low emission vehicle standards. Significant precious metal cost saving has been achieved.

Generally, Pd-based TWCs possess several advantages compared to the Pt/Rh catalysts. Economical consideration was the initial driving force to use

Pd. Pd is by far the most abundant noble metal that can be utilized in automobile exhaust gas treatment. Pd-based TWCs also give a faster light-off, which leads to an overall improvement of the performance particularly for the HC conversion (30,31). Compared to Pt-based ones, Pd catalysts were shown to adsorb much more oxygen over a wide temperature range (32), which influences the oxidation ability significantly. Furthermore, Pd metal is known to have better resistance to thermal sintering than Pt and Rh (33). Therefore, it was considered as a promising component in high temperature applications. The main limitations for the application of Pd are the high sensitivity to the poisoning by sulfur and lead (34,35). However, as the improvement of the fuel quality, lead levels are close to zero at present and fuel sulfur levels have also been markedly reduced. Consequently, the limitation for Pd-only catalyst is much less severe than that in the early time and most of the modern TWCs are based on Pd containing formulations (36). However, compared to Pt/Rh catalyst, Pd shows intrinsically lower activity for NOx reduction and saturated hydrocarbon oxidation (37,38). The self-poisoning by hydrocarbon molecules is the cause of the poor NOx reduction capability of the Pd catalysts (39). Therefore, it is necessary to enhance the hydrocarbon oxidation activity in order to improve NOx conversion efficiency in a fuel-rich region. In this article, the developments of Pd-based TWCs is reviewed, with focusing on the catalyst system, reaction mechanism, and kinetics as well as perspectives to the future.

2. STATE OF PALLADIUM IN THE REACTION

The performance of the Pd-based catalyst strongly depends on the chemical state of Pd during the reaction. Fernández-García et al. (40) investigated the state of Pd over Pd/Al_2O_3 and Pd/CeO_2-ZrO_2 TWCs under the stoichiometric simulated gas (C_3H_6+CO+NO+O_2+N_2 or CO+NO+O_2+N_2). The in-situ diffuse reflectance infrared Fourier transform spectroscopy (DRIFTS) and X-ray absorption near edge structure (XANES) results indicated that the initially fully oxidized Pd is reduced to Pd(0) over Pd/Al_2O_3 with the increase of reaction temperature. However, the presence of CeO_2-ZrO_2 stabilizes the Pd species with average oxidation state as Pd (I) which retains a certain metallic-like character due to the existence of Pd-Pd bonds. The presence of C_3H_6 in the reactant gas also contributes to the stabilization of Pd (I). The Pd (I) species is proved to be beneficial to the three-way reaction, especially for the CO and C_3H_6 removal. Another work of the same group further confirmed that the presence of CeO_2-ZrO_2 retards the reduction of Pd under the dynamic conditions (41). Recently, Lu et al. (42) examined the state of Pd over a Pd/CeO_2-ZrO_2-Al_2O_3 catalyst. The reaction was performed under a simulated transient cycles conditions with changed reaction temperatures (100–900°C) and fluctuating oxygen conditions (7000 ppm CO, 150 ppm C_3H_6, 1600 ppm

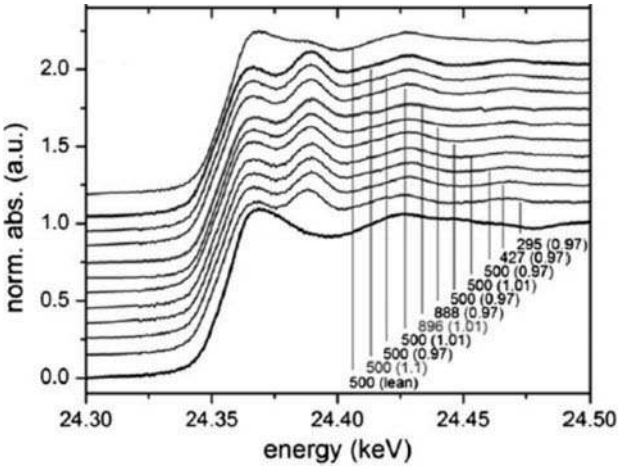

Figure 2: Operando XANES spectra at the Pd K-edge recorded on Pd/ACZ during the simulated driving cycle. The bottom spectrum in each panel corresponds to room temperature in $\lambda = 0.97$. Values in brackets indicate the λ value. Reprinted from (42) with permission of Elsevier Science Publishers B.V.

NO, 2650–3025 ppm O_2 and He balance), which is more close to the realistic conditions than that in (40). The in situ XANES results (Fig. 2) demonstrate that the fresh catalyst with fully oxidized Pd is quickly reduced to the metallic Pd, and this Pd (0) species remains within the whole temperature range regardless of the air/fuel ratio. Only significantly oxidizing conditions (with $\lambda \gg 1$) can cause the re-oxidation of Pd, as shown in the top spectrum of Fig. 2. However, as the X-ray absorption spectroscopy method is sensitive to the bulk phase of catalyst, the re-oxidation of the surface Pd during the transient cycles cannot be excluded in this work. A strong dependence of Pd chemical state on the particle size under the cycling conditions was observed by Iglesias-Juez et al. (43). They prepared two Pd/Al_2O_3 catalysts (Pd metal loading 2 wt% and 4 wt%) and estimated an average particle size of about 1.5 and 3.0 nm for 2 wt% Pd/Al_2O_3 and 4 wt% Pd/Al_2O_3, respectively. The reaction was performed under cycling conditions with 5% CO and 5% ($NO+O_2$; 1:4.5) gas mixtures in He, with 10 repetition of 13.65 × 2 s. They found that both Pd (0) and Pd (I) can be present upon the CO reducing step of the CO/($NO+O_2$) cycle, but it is strongly dependent on the particle size of the Pd. Pd (I) is the main species for 2 wt% Pd/Al_2O_3 with about 1.5 nm particle size while Pd (0) dominates the reaction for 4 wt% Pd/Al_2O_3 with around 3.0 nm particle size. The Pd (I) species shows a higher activity towards CO elimination than the Pd (0).

Although the fully oxidized Pd can be the active phase for a fresh catalyst, the continuous existence of reduced Pd should be considered during the real working conditions. The state of the reduced Pd as Pd (0) or Pd (I) is influenced by the particle size of Pd and the support material. Generally,

small particle size of Pd and the presence of CeO_2-ZrO_2 OSC material favors the presence of Pd (I) species which has high activity towards the three-way reaction, especially for the elimination of hydrocarbon and carbon monoxide.

The loading amount of Pd in the Pd-based TWC is a deeply concerning factor in industry. Brisley et al. (44) investigated the effect of Pd loading on the three-way performance of the Pd-only catalyst. The results indicated that the HC and CO conversions are good at moderate Pd loadings while NO*x* conversion increases sharply with the palladium loading. This conclusion is in line with that of Hu et al. (45), suggesting negligible effect of Pd loading on HC and CO conversion performance but better performance in NO*x* conversion at higher Pd loading levels. Summers et al. (30) tested the influence of the palladium loading on the integral HC conversion and the HC light-off performance. The results indicated that with the increase of Pd loading from 0.68 g/L to 17.0 g/L, the integral HC conversion increases from 91% to 97% while the HC light-off (50% conversion) temperature drops from 420°C to 305°C. The improvement in the integral HC conversion performance with the increase of the palladium content is relatively small, compared to the improvement in the HC light-off performance. Kang et al. (46) investigated the effect of Pd loading with making six Pd-based TWCs containing 20, 80, 140, 160, 200, and 240 g/ft^3 Pd. They measured the Pd metal surface area (MSA) with CO chemisorptions and thought the MSA can be used as an index of the performance of the catalyst. They found that the Pd MSA increased linearly with the Pd loading in the range of 20–80 g/ft^3. However, the rising trend exhibits a nonlinear increase with the further increase of Pd loadings. Then no appreciable difference in the Pd MSA for the Pd loading range in 160 g/ft^3 and 240 g/ft^3 was observed. Furthermore, they proposed an empirical model between the catalyst activity function (α) and Pd loading (L):

$$\alpha = 1.05 - 1.08 \exp\left(\frac{-2.0-L}{70.0}\right) \tag{10}$$

in which α is defined as the ratio of Pd MSA at a given loading to Pd MSA at 240 g/ft^3 Pd loading. This model well predicts the increase trend of Pd MSA over a wide range of Pd loadings (see Fig. 3). A common tendency is observed that the emissions are lowered as the Pd loading increased to some extent, due to the increased number of active sites (47). However, the use of high Pd loading means much high cost on catalyst. In addition, the reduction of NO*x* requires the presence of CO, HC, or H_2. If the rates of the oxidation of these species are very rapid, as happens over the catalyst with a high density of active Pd sites, the partial pressure of these species will be too low and the conversion of NO*x* on the catalyst will be limited (44). Furthermore, high Pd loading favors sintering at high temperatures, which leads to the deactivation of the TWC.

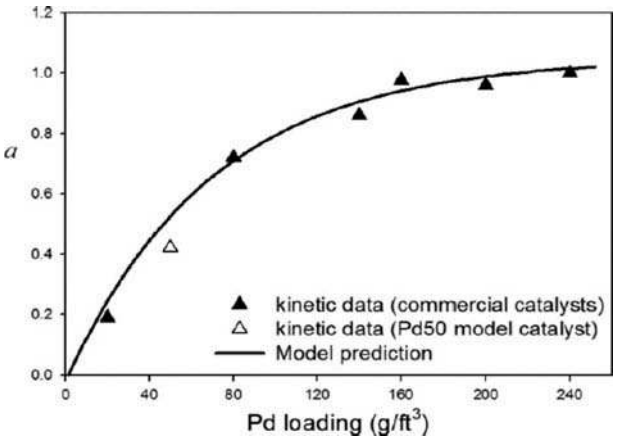

Figure 3: Model prediction of catalytic activity by using activity function (α). α is defined as the ratio of Pd MSA at a given loading to Pd MSA at 240 g/ft^3 Pd loading. MSA: metal surface area. Reprinted from (46) with permission of Elsevier Science Publishers B.V.

3. FUNCTIONS OF CATALYTIC COMPONENTS

3.1. Support and Oxygen Storage Materials

3.1.1. Al_2O_3

The most frequently used TWCs are composed of noble metals supported on an alumina coated ceramic monolith (8). Due to the fact that the honeycomb monolith has a low surface area (about 3m^2/l) (36), the application of an interlayer alumina aims at providing a high surface area for enhancing the dispersion of the noble metals. Mamede et al. (48) compared the performance of bulk Pd and 1wt% Pd/Al_2O_3 for CO+NO reaction and found the reaction rate over latter one is much higher than on bulk Pd. This was attributed to the great difference of dispersion between bulk Pd (1.4%) and 1wt% Pd/Al_2O_3 (40%). In addition to the high surface area and the relatively good hydrothermal stability under the vehicle exhaust condition, the interlayer, behaving as the primary support for the noble metals, should prevent the catalyst components from sintering (49,50). In most of the cases, γ-Al_2O_3 is employed due to its high surface area. However, in some of the other cases other alumina phase such as θ-Al_2O_3 can also be found, especially for the high temperature applications such as in the close coupled catalysts (CCCs) where the temperature reaches 1000°C. θ-Al_2O_3 has a better thermal stability than γ-Al_2O_3 (9). A temperature of 1000°C transforms γ-Al_2O_3 into α-Al_2O_3 which has a typically low surface area (50). As a result, stabilization of the transition alumina phase is necessary for the TWCs. Shen et al. (51) prepared a Pd-only catalyst loaded on the P-doped Al_2O_3 prepared by sol-gel method. They found that the Pd/P-Al_2O_3

catalyst gives much higher BET surface area and three-way performance than the Pd/Al_2O_3 catalyst after 1050°C for 10 h under 10% steam in air. The interaction between Pd clusters and P-O-Al units in the P-doped Al_2O_3 prevents the sintering of Pd and the phase segregation of $AlPO_4$ in γ-Al_2O_3.

CeO_2 has been proved to be effective to improve the thermal stability of Al_2O_3. Ozawa and Kimura (52) compared the thermal stability of a series of $xCeO_2/Al_2O_3$ (x = 0.5, 1, 2, 3, 5, and 10 mol%) material through a high temperature aging at 1000–1200°C in air for 5 h. They found that the thermal stability of Al_2O_3 is improved with the addition of only 0.5–2 mol % CeO_2. The X-ray diffraction (XRD) characterization (see Fig. 4) showed that a pure Al_2O_3 completely transformed to α-Al_2O_3 during the calcination in air at 1200°C, while the Al_2O_3 with doping 0.5 mol% CeO_2 still retained the structure of θ-Al_2O_3. The XRD peaks of CeO_2 phase appear only in the patterns of the Al_2O_3 samples when the CeO_2 content is more than 2 mol %. This result indicates that the addition of CeO_2 improves the thermal stability of γ-Al_2O_3, but its overload leads to the formation of segregated CeO_2 particles. Shyu et al. (53) proposed the formation of a $CeAlO_3$ phase because they measured a Ce (III)-like X-ray photoelectron spectrum (XPS) and a completely different Raman spectrum from that of CeO_2 in a 7 wt % CeO_2/Al_2O_3 sample, which was heated

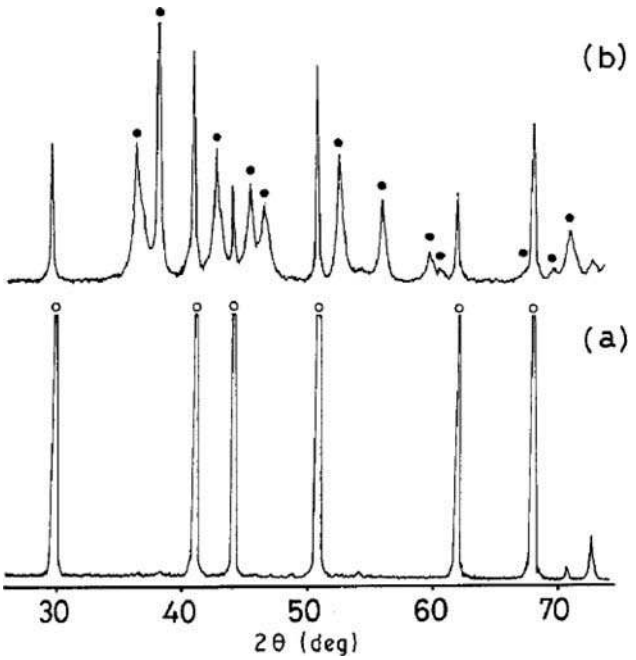

Figure 4: XRD patterns of (a) pure Al_2O_3 and (b) 0.05 mo1% Ce-Al_2O_3. Both samples were calcined in air at 1200°C for 5 h before test. (●): θ-Al_2O_3; (O): α-Al_2O_3. Reprinted from (52) with permission of Springer.

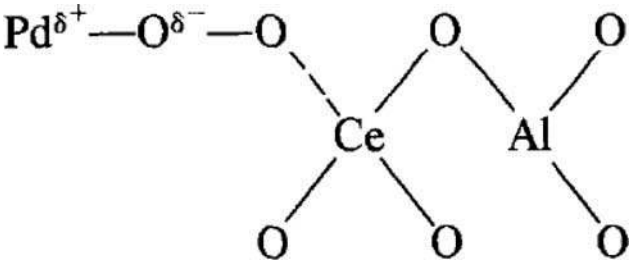

Figure 5: The schematic diagram of surface complex in $Pd/CeO_2/Al_2O_3$ system. Reprinted from (55) with permission of Elsevier Science Publishers B.V.

at 1000°C for 80 h in flowing 10% H_2/Ar. The formation of $CeAlO_3$ phase was believed to be related to the good thermal stability of the CeO_2/Al_2O_3 material. Piras et al. (54) also assumed that the promotion effect of CeO_2 on the thermal stability of γ-Al_2O_3 is due to the formation of $CeAlO_3$ which inhibits the crystal growth of α-Al_2O_3. However, this effect cannot be observed under reducing or redox conditions at 1200°C. Shyu et al. (55) proposed that Pd accelerates the reversible reaction of $CeO_2/Al_2O_3 \longleftrightarrow CeAlO_3$ and presented a model to explain the experimental observations (see Fig. 5). In this system, Pd is in a state between Pd° and PdO. PdO may form solid solution with $CeAlO_3$ and the solution may transform to Pd° and $CeAlO_3$ in a reduction atmosphere, while the reoxidation results in the formation of PdO and CeO_2. Pd assists this redox process and moderates the loss of OSC owing to the $CeAlO_3$ formation which inhibits the $Ce^{4+} \longleftrightarrow Ce^{3+}$ redox reaction and maintains the high OSC of CeO_2 as a result.

In addition to CeO_2, some other oxides, such as La_2O_3 and BaO, have also been found to enhance the thermal stability of Al_2O_3. Burtin et al. (56) investigated the kinetics of the transformation from γ-Al_2O_3 to α-Al_2O_3 and found that the addition of La_2O_3 significantly lowers the rate of the transformation of Al_2O_3 calcinated at high temperatures. Yamamoto et al. (57) confirmed the positive effect of La_2O_3 addition on the thermal stability of γ-Al_2O_3. They found that the addition of La_2O_3 to γ-Al_2O_3 poisons the original strong acid sites and generates other weaker Lewis acid sites over Al_2O_3. The change of strong Lewis acid sites on Al_2O_3 suppresses the hydrolysis-dehydration scheme, inhibiting the phase transformation from δ to α-phase. Kwak et al. (58) examined the influence of incorporation of La_2O_3 and BaO on the phase transformation of γ-Al_2O_3 and found that both the two additives retard the phase transformation of Al_2O_3 from γ to α-phase after calcination at 1000°C for 10 h. They observed that the addition of La_2O_3 and BaO favors the conversion of pentacoordinated aluminum into octahedral ones. The presence of pentacoordinated aluminum is closely related to the thermal instability of γ-Al_2O_3 at high temperatures.

3.1.2. CeO_2

TWCs work efficiently with achieving simultaneous conversions of CO/HC/NO*x* only at the air fuel ratios close to the stoichiometric point. However, fluctuations between fuel-rich (net reducing) and fuel-poor (net oxidizing, also called lean burn condition) conditions severely decrease the efficiency of the catalysts (5). In the beginning of 1980s, CeO_2 was found have a significant OSC, while Al_2O_3 was realized do not store and release oxygen under the vehicle exhaust gas convertor conditions (59).

There is no doubt that the presence of CeO_2 in the support layer enhances the performance of the Pd-based TWCs under real exhaust conditions because of the OSC of CeO_2 (60,61). Furthermore, the interface between Pd and CeO_2 has a positive contribution to the three-way reactions. Sanchez and Gazquez (62) proposed that the metal atoms may anchor into the oxygen vacancies formed at the surface of the CeO_2, leading to the occurrence of a "nesting" effect, while the diffusion of the metal atoms into the bulk phase of CeO_2 is difficult due to the high barrier caused by the cationic sublattice. The interface between metal and CeO_2 can provide new sites for the reaction. Holles et al. (63) compared the performance of Pd/Al_2O_3 and $Pd/CeO_2/Al_2O_3$ catalyst prepared by step-wise impregnation technique under the stoichiometric conditions. They found that the addition of CeO_2 to the Pd/Al_2O_3 catalyst increases the reaction rate of NO reduction by CO for at least one order of magnitude (see Fig. 6). They believed that CeO_2 provides new active sites at the Pd-CeO_2 interface to enhance the NO + CO reaction through facilitating the NO dissociation which may be the rate-limiting step of the reaction. This conclusion

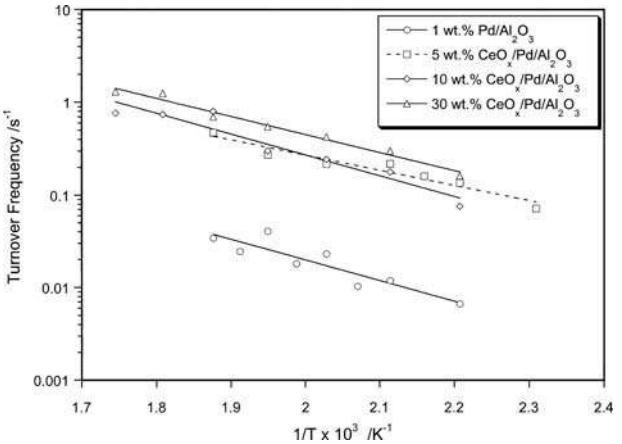

Figure 6: Arrhenius-type plots for the NO+CO reaction over 1.0 wt% Pd/Al_2O_3, 5 wt% CeO*x*/Pd/Al_2O_3, 10 wt% CeO*x*/Pd/Al_2O_3, and 30 wt% CeO*x*/Pd/Al_2O_3. Reaction conditions: 5.07 kPa NO+5.07 kPa CO + He balance, Total pressure in the reactor was 1 atm. Reprinted from (63) with permission of Elsevier Science Publishers B.V.

was also supported by Ciuparu et al. (64) who found that the pre-reduced Pd-CeO_2/Al_2O_3 catalyst is more active for NO reduction than the pre-reduced Pd/Al_2O_3 sample. They compared the NO-TPD results of four pre-reduced catalysts, i.e., a CeO_2/Al_2O_3 sample prepared with an impregnation technique and three Pd-CeO_2/Al_2O_3 catalysts prepared with coimpregnation, successive impregnation, and co-grafting methods, and observed that the Pd-CeO_2/Al_2O_3 catalysts prepared with coimpregnation and successive impregnation methods exhibit higher selectivity for N_2 than the other two samples. They suggested that the active sites for NO dissociation are located at the Pd-CeO_2 boundary rather than on the Pd or CeO_2 surfaces. The interaction between Pd and CeO_2 was found significantly enhance the OSC and the DOSC of the catalyst (65,66). The drop of the activation energy for the migration of lattice oxygen migration by the loading of Pd on the CeO_2 was found to be the main reason for this phenomenon (67). Descorme et al. (68) believed that the Pd-CeO_2 couple provides high mobility of oxygen at the metal-oxide interface (see Fig. 7), thus facilitating the DOSC.

3.1.3. CeO_2-ZrO_2

Since 1995, pure CeO_2 has been gradually replaced by the CeO_2-ZrO_2 mixed oxides in the TWCs (9). The main limitation for the application of pure CeO_2 is the poor thermal stability because the vehicle exhaust condition is thermally hash. With the reaction temperature higher than 800°C, the catalyst with pure CeO_2 in the support experienced deactivation seriously. The deteriorations of the catalyst due to sintering include the loss of the surface area and OSC (69). In addition, the metal-CeO_2 interaction is also weakened (59).

Extensive efforts have been made on improving the thermal stability of CeO_2. Among these efforts, the incorporation of ZrO_2 into the CeO_2 lattice has been proved to be effective in preventing CeO_2 from sintering (70,71). Cuif

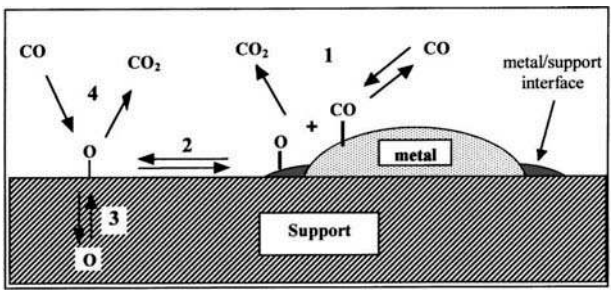

Figure 7: Schematic representation of possible processes involved during OSC measurements in NM/CeO_2 systems. Oxygen transfer from the support to the metal surface depends on oxygen mobility at the surface, in the bulk of the oxide and on the metal/support interface. CO direct oxidation on the support is assumed to be very low. Reprinted from (68) with permission of Elsevier Science Publishers B.V.

et al. (72) found that the CeO_2-ZrO_2 mixed oxide in an appropriate composition range retains a high surface area and OSC even after calcination at 900°C for 6 h. Di Monte et al. (50) compared the thermal stability of CeO_2/Al_2O_3 and CeO_2-ZrO_2/Al_2O_3 prepared by wet impregnation. They measured the OSC of the material after an experiment in which the material was reduced in H_2 with a ramping of the temperature up to 1000°C and then was re-oxidized fully at 427°C in 5% O_2 in Ar. They found that the formation of $CeAlO_3$ in CeO_2/Al_2O_3 leads to a decrease of the OSC, while no formation of $CeAlO_3$ was detected in the CeO_2-ZrO_2/Al_2O_3 samples. Moreover, the stabilization effect depends on the amount of ZrO_2 added to CeO_2. After calcination at 1100°C for 5 h, a sample $Ce_{0.2}Zr_{0.8}O_2/Al_2O_3$ gives much smaller CeO_2-ZrO_2 average crystallite (7 nm) and much higher surface area (115 m^2/g) than that of CeO_2 in the CeO_2/Al_2O_3 sample (20 nm and 60 m^2/g). Fernández-García et al. (73) made a similar comparison between CeO_2/Al_2O_3 and CeO_2-ZrO_2/Al_2O_3 prepared by microemulsion method and observed through the transmission electron micrograph (TEM) technique that the average particle size of CeO_2 in CeO_2/Al_2O_3 (ca. 20 nm) is twice of that of the CeO_2-ZrO_2 in CeO_2-ZrO_2/Al_2O_3 (ca.10 nm) after the thermal treatment in air at 1000°C for 12 h. Such promotion effect of ZrO_2 to CeO_2 was also confirmed by Ozawa et al. (74). The good thermal stability of the catalyst with CeO_2-ZrO_2 as the support is related to the formation of solid solution between CeO_2 and ZrO_2 (59,74). Granger et al. (75) compared the activity of the catalysts with Pd supported on the supports with different Zr/Ce ratio, i.e., $Zr_xCe_{1-x}O_2$ (x = 0, 0.25, 0.5, 0.75, 1) and their results showed that the initial activity of the catalyst is dependent on the Ce content. The catalyst with the highest initial activity was Pd/CeO_2, however, this catalyst experienced a fast deactivation during the running at 400°C. The catalyst $Pd/Zr_{0.25}Ce_{0.75}O_2$ was proved to be the most resistant one to deactivation, suggesting that the incorporation of Zr to CeO_2 improves the stability of the Pd-based catalyst.

Jen et al. (76) measured the OSC of a Pd/CeO_2-ZrO_2 and a Pd/CeO_2 catalyst with a cyclic redox aging technique for 12 h. The aging process was carried out at 1050°C by alternatively switching the reducing and oxidizing feed gas every 10 min. They found a remarkably improvement of the value for the Pd/(70 wt% CeO_2-ZrO_2) over the Pd/CeO_2 catalyst. Measured at different temperatures, the CeO_2-ZrO_2 supported catalyst gave an OSC from 7–140 times higher than that of the pure CeO_2 supported one under the same testing condition. The increased OSC of CeO_2-ZrO_2 was attributed to the defective sites formed because of the incorporation of Zr into the CeO_2 lattice. These defects greatly enhance the transport of oxygen from the bulk to the surface of CeO_2 (24,77). Balducci et al. (78,79) investigated the bulk reduction and oxygen migration in the CeO_2-ZrO_2 with a computer simulation technique and found that the introduction of ZrO_2 into the CeO_2 lattice lowers the energy barrier for Ce^{4+} reduction and increases the mobility of the lattice oxygen (see Fig. 8),

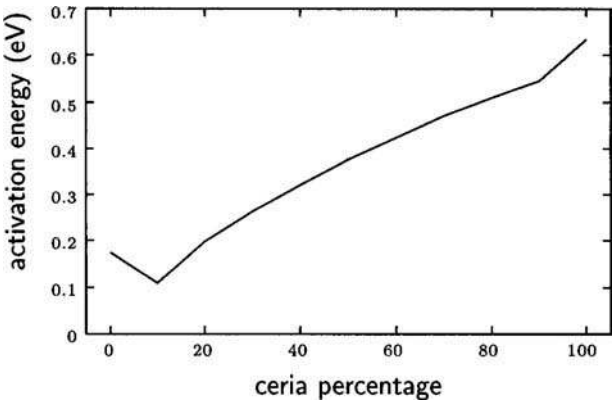

Figure 8: Activation energy for oxygen migration as a function of CeO_2 content in Ce-Zr mixed oxides obtained by the computer simulation. Reprinted from (78) with permission of American Chemical Society.

as well as the diffusion rate of oxygen from the bulk to the surface, thus promoting the redox circle of the Ce^{4+}/Ce^{3+} couple. This result is consistent with the observations of Graham et al. (80) and Fornasiero et al. (81), they both found that the addition of ZrO_2 has a promotion effect on the reducibility of CeO_2. Furthermore, H_2-temperature programmed reduction (H_2-TPR) results indicated that the oxygen reduction occurs at the surface and in the bulk phase of CeO_2-ZrO_2 simultaneously at low temperatures. While the H_2-TPR peaks, related to surface and bulk oxygen reduction, appear separately for the pure CeO_2 sample (81).

The robust of the surface area of CeO_2 in high temperature is an essential factor for smoothing the Ce^{4+}/Ce^{3+} redox cycle and maintaining a high value of OSC. The loss of the CeO_2 surface area dramatically reduces the amount of oxygen available from CeO_2 (69). However, Kašpar and his coworkers (82,83) got different experience with CeO_2-ZrO_2 and found that the maintenance of a high OSC of CeO_2-ZrO_2 after redox aging is irrespective to a significant loss of the surface area. They suggested that the OSC of the CeO_2-ZrO_2 material is independent on the textural properties. Fernandes et al. (84) also found that the CeO_2-ZrO_2 material exhibits a high OSC in spite of the severe sintering due to the aging at 1200°C for 72 h, which means that the bulk property dominates the OSC rather than the surface parameters. Jen et al. (76) observed a different feature between a Pd/CeO_2-ZrO_2 and a Pd/CeO_2 catalyst that a new H_2-TPR peak (Fig. 9) appears between 100°C and 200°C for the CeO_2-ZrO_2 supported catalyst after 1050°C (even 1150°C) redox aging, which is totally absent in Pd/CeO_2. They believed that this new peak accounts for a large part of available oxygen in the aged sample, which may be a reasonable explanation for the superior OSC of CeO_2-ZrO_2 after high temperature treatment. The generation of such easily reducible sample was considered to play the key role in

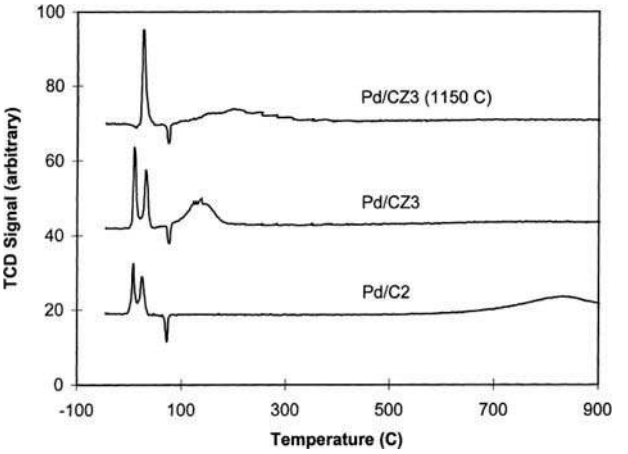

Figure 9: H_2-TPR traces of 1050°C redox-aged 2% Pd on C2 (100% CeO_2) and CZ3 (70% CeO_2/30% ZrO_2) catalysts and 1150°C redox-aged 2 wt% Pd on CZ3 (70% CeO_2/30% ZrO_2) catalyst. The redox aging process was carried out for 12 h by alternating the gas mixture containing 1 mol% CO/H_2 (molar ration 3:1) with 0.5 mol% O_2 every 10 min. The rest of the gas mixture consisted of 0.002 mol% SO_2, 10 mol% H_2O and N_2 balance. Reprinted from (76) with permission of Elsevier Science Publishers B.V.

the retaining of the OSC in aged sample. Fernández-García et al. (73) reported a similar phenomenon that a new H_2-TPR peak at around 380°C appeared for the aged CeO_2-ZrO_2/Al_2O_3 sample which is absent for the non aged one. These results suggest that the CeO_2-ZrO_2 shows excellent OSC performance even under severe sintering due to the appearance of new oxygen species in the aged sample. This is essential for the preservation of the performance of Pd catalysts during long-term application.

Fernández-García et al. (85,86) compared the activity of Pd catalyst supported on $Ce_xZr_{1-x}O_2$ and $Ce_xZr_{1-x}O_2$/Al_2O_3 prepared by microemulsion method for NO reduction and CO oxidation under stoichiometric conditions. For NO reduction, a clearly superior activity of Pd supported on $Ce_xZr_{1-x}O_2$/Al_2O_3 to those supported on $Ce_xZr_{1-x}O_2$ and Al_2O_3 is achieved, while Pd/$Ce_xZr_{1-x}O_2$ catalyst shows better performance than others for CO oxidation. The most active sites for CO oxidation involve Pd interacting with $Ce_xZr_{1-x}O_2$ entities (86). Another work of the same group (87) investigated the influence of Pd-(CeO_2-ZrO_2) interface on the performance of the catalyst under dynamic CO/NO cycles. Two Pd/Al_2O_3 catalyst with or without CeO_2-ZrO_2 and having a similar Pd particle size were prepared. A much higher activity for converting CO and NO was observed on CeO_2-ZrO_2 sample. They believed that the Pd-(CeO_2-ZrO_2) interface appears as the new center for CO and NO dissociation and promotes N_2 and CO_2 formation. This interface has also been found to change the pathway for NCO formation and facilitate the evolution of NCO into CN, which may influence the N_2 production.

The results mentioned indicate that the interaction between Pd- and CeO_2-based OSC plays a dominant role in three-way catalysis. This interaction leads to a significantly beneficial synergism which further promotes the OSC and DOSC of the CeO_2-based material and stabilizes the Pd with high dispersion. The interface of Pd-(CeO_2-based material) also provide new sites for removal of the pollutants in the exhaust gas. More importantly, the interaction between Pd and CeO_2 stabilizes the active Pd (I) species under the dynamic conditions due to the oxygen transfer effect occurring at the interface, which helps to maintain the high performance of the Pd-based catalyst under the working conditions.

3.2. Promoter

3.2.1. Promoter for Catalyst without CeO_2-ZrO_2

In order to improve the three-way performance, especially for the NO reduction activity and the stability of the Pd-based catalyst, much attention has been paid to modify the catalyst with suitable promoters. As the effectiveness of ZrO_2 in promoting the performance of CeO_2 in TWCs was not openly presented by the industrial researchers until the year of 1997 (59), a lot of early works were focus on the TWCs without CeO_2-ZrO_2 mixed oxides.

The reaction conditions of different promoters for Pd-catalysts without CeO_2-ZrO_2 were summarized in Table. 1. Skoglundh et al. (88) investigated the introduction of La_2O_3 to the Pd/Al_2O_3 catalyst prepared by stepwise impregnation method and got almost 100% conversion of NO under a reducing condition in the range of λ ($\lambda = (2(O_2)+(NO)/((CO)+9(C_3H_6)))$ from 0.7–1.0. They explained this superior NO conversion over the $Pd/La_2O_3/Al_2O_3$ catalyst to the Pd/Al_2O_3 with the formation of a Pd-La oxide which favors the reaction of NO reduction by CO. Logan and Graham (89) studied the NO chemisorption on Pd (100) with over-layers of La_2O_3 and Al_2O_3. The results indicated that NO was partially dissociated on La_2O_3 but was not dissociative on Al_2O_3 at 27°C, which suggests that La_2O_3 enhances the dissociative adsorption of NO on Pd surface. Muraki et al. (39,90) also confirmed the positive effect of La_2O_3 in the Pd-based catalyst. They believed that the addition of La_2O_3 weakens the chemisorption strength of hydrocarbons on Pd, which effectively enhances the reduction of NO. A Schematic Scheme was proposed by Shinjoh (91) to show the effect of La_2O_3 addition to Pd catalyst (Fig. 10). In another work of Muraki et al. (92), the high activity of NO reduction over the Pd-La_2O_3/α-Al_2O_3 catalyst under stoichiometric and reducing condition is attributed to the high activity of La_2O_3 for steam-reforming and WGS reactions that supply H_2. NO reduction by H_2 is fast and highly selective.

Adams and Gandhi (93) examined the introduction of WOx into a Pd/Al_2O_3 through a stepwise impregnation method and found that the addition of WOx

Table 1: The reaction conditions of different promoters for Pd-catalysts without CeO_2-ZrO_2.

Reference	Promoter	Reaction temperature (°C)	Reaction gas composition	λ value [a]
Skoglundh et al. (88)	La_2O_3	450	1000 ppm NO+1.6% CO+300 ppm C_3H_6 +0.6–0.89% O_2+N_2	0.7–1.0
Muraki et al. (90)	La_2O_3	350	NO+CO+C_3H_6+C_3H_8+O_2+3%H_2O+10% CO_2+N_2	0.65
Muraki et al. (92)	La_2O_3	500	1000 ppm NO+1.5% CO+1500 ppm C_3H_6 0.5% H_2+0.6–3.2% O_2+3% H_2O+12% CO_2+N_2	0.6–1.0
Adams and Gandhi (93)	WOx	550	1000 ppm NO+1.5% CO+1000 ppm C_3H_6+ 500 ppm C_3H_8+0.5% H_2+1% O_2+ 20 ppm SO_2+N_2	0.625
Schmal et al. (96)	MoOx	220–350	0.6% NO+1.3% CO+He	0.46
Noronha et al. (97)	MoOx	220	0.6% NO+1.0% CO+He	0.6
Neyertz and Volpe (98)	VOx	25–400	400 ppm NO+400 ppm CO+He	1.0
Kim and his coworkers (38,99)	VOx, ZrO_2	150–400	1500 ppm NO+0.6% CO+500 ppm C_3H_6+ 0.3% H_2+0.6% O_2+30ppm SO_2+13% H_2O+N_2	1.0
Yentekakis et al. (100)	Na_2O	380	1% NO+0.8% C_3H_6+He	0.14
Sekiba et al. (102)	BaO La_2O_3	480	Engine test	≤1.0
Kobayashi et al. (104)	BaO, SrO La_2O_3	400	Engine test	Around 1.0

[a] $\lambda = \frac{2[O_2]+[NO]}{[H_2]+[CO]+9[C_3H_6]+10[C_3H_{10}]}$.

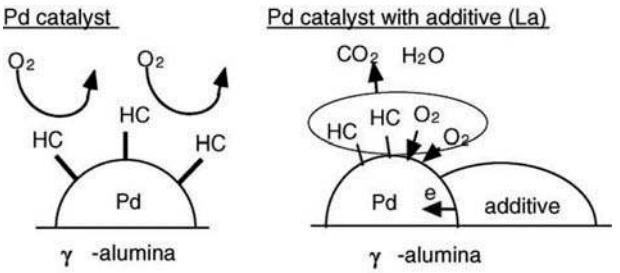

Figure 10: Schematic scheme demonstrating the effect of La_2O_3 addition to Pd/Al_2O_3 catalyst. La_2O_3 addition weakens the adsorption strength of Pd with HC by a moderate electron supply and favors HC oxidation. Reprinted from (91) with permission of Elsevier Science Publishers B.V.

decreases the NO conversion but increases the selectively to N_2, e.g., the NO conversion and selectivity to N_2 at 550°C for the Pd-WOx/Al_2O_3 are 37% and 95%, respectively, while those are 71% and 69%, respectively, for the Pd/Al_2O_3 catalyst. Halasz and Brenner (94) tested the performance of a Pd-$MoOx/Al_2O_3$ catalyst containing 2 wt% Pd and 20 wt % MoOx and found that MoOx promotes the activity and selectivity for the reduction of NO by CO, H_2 and also the mixture of $CO+H_2$ in the temperature range of 300–550°C, under either slightly reducing or slightly oxidizing conditions. Moreover, the NO removal activity of this catalyst exceeds slightly that of a commercial Pt-Rh catalyst under oxidizing conditions in the atmosphere of $NO+CO+H_2+O_2$. However, the sublimation of MoOx at high temperatures is a problem for the catalyst with such a high MoOx content (95). Schmal and his coworkers (96,97) investigated a Pd-$MoOx/Al_2O_3$ catalyst containing 1 wt% Pd and 8 wt% MoOx for the reaction of NO reduction by CO. The results showed that this catalyst is much more active and selective to N_2 than the catalysts of Pd/Al_2O_3 and $MoOx/Al_2O_3$. Mo was found reduce to Mo^{4+} at low temperatures in the presence of Pd particles, and the NO-TPD technique provides evidence for NO dissociation over these partially reduced Mo oxides. They assumed the enhancement of NO reduction is due to the modification of the electronic properties of the Pd particle by the partially reduced Mo oxide. The formation of the new adsorption sites between Pd and partially reduced Mo oxide decreases the stability of the atomic N on the surface of Pd and promotes the NO dissociation.

Neyertz and Volpe (98) examined the effect of VOx addition into a Pd/Al_2O_3 catalyst and got a higher N_2 selectivity in CO+NO reaction especially at low temperatures. They proposed that VOx weakens the N-O bond and favors its dissociation, thereby facilitating N_2 formation at low reaction temperatures. Kim and his-coworkers (38,99) tested the effects of VOx and ZrO_2 contents on the performance of a Pd-VOx-ZrO_2-Al_2O_3 catalyst prepared with a sol-gel method with a simulated gas feed containing 30 ppm SO_2. The results showed that VOx is a promoter for enhancing the resistance against SO_2 and

Zr is the one for improving the activity and thermal stability. However, the catalyst which has a mole ratio of V/Zr = 0.36 shows both a good durability against SO_2 and a high thermal stability. They think that there is a synergistic interaction between VOx and ZrOx in this Pd-only catalyst due to the formation of a tetrahedrally coordinated V species which was confirmed by ^{51}V solid-state Nuclear Magnetic Resonance spectrum, like $(V\text{-}O)_3V = O$, inhibiting the crystal growth of PdO and the phase transformation of ZrOx, and γ-Al_2O_3 during the thermal aging process.

Alkali metal and alkali earth metal oxides such as Na_2O, K_2O, and BaO have been proved beneficial to the performance of the Pd-only catalyst (100–102). Yentekakis et al. (100) measured the effect of Na_2O content in a Pd/YSZ catalyst on NO reduction by C_3H_6. Their results suggested that the addition of 0.068 wt% Na_2O increases the reaction rate significantly and the maximum selectivity of N_2 rises from around 75% on the unpromoted catalyst to about 95% on the promoted one, while further increase of the Na_2O content leads to the poisoning of the catalyst. They proposed that the role of Na_2O is to enhance the NO chemisorption while weakening that of C_3H_6 which is much stronger than that of NO on the Pd surface. However, too much Na_2O blocks the surface of Pd and inhibits the adsorption of the reactants. Shinjoh et al. (103) confirmed the promoting effect of alkaline metal oxides (Li, Na, K, Cs,) due to the weakening of the adsorption strength of C_3H_6 on Pd. XPS analysis results indicated that this phenomenon is caused by the increase of the electron density of the Pd particles. The addition of BaO and La_2O_3 to a $Pd/CeO_2/Al_2O_3$ catalyst was proved to enhance the NO conversion under reducing conditions, especially after 850°C aging for 30 h (102). Kobayashi et al. (104) compared the effects of the incorporation of BaO, SrO, and La_2O_3 into the Pd/Al_2O_3 on the three-way performance of catalyst and found that all these promoters improve the performance of the Pd-only catalyst. This improvement effect decreases as the increase of the electronegativity of the added cations, as shown in Fig. 11. They also observed with XPS technique that the electron density around Pd (II) increased due to the addition of BaO. They believed that the Pd (II) (with an electron structure of Kr ($4d^8$)) in $Pd/BaO/Al_2O_3$ have an electron configuration similar to that of Rh Kr ($4d^85s^1$).

3.2.2. *Promoter for CeO_2-ZrO_2*

The OSC materials play an important role in the Pd-based catalyst for the three-way reactions. For the purpose of increasing the thermal stability and OSC of the widely used CeO_2-ZrO_2 mixed oxide, promoters were introduced into the support. Zr-Ce-Pr-O and Zr-Ce-Nd-O mixed oxides were found have high oxygen mobility at low temperatures, therefore these materials were thought promising to be used as the OSC material in TWCs (105,106). Wu et al. (107) investigated the addition of Pr and Nd oxides on the structure and the

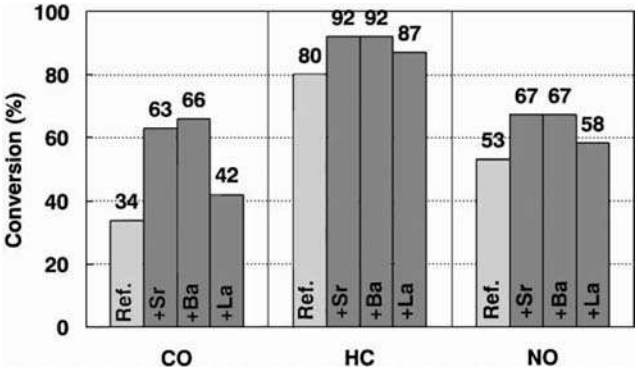

Figure 11: Effect of the promoters (Sr, Ba, and La oxide) on three-way catalytic performance of Pd-based catalyst. The evaluations were conducted around the stoichiometric air/fuel ratio (A/F = 14.5–14.7) at a catalyst inlet temperature of 400°C, space velocity 68,000 h^{-1}. The catalyst was aged for 50 h on the engine dynamometer at the catalyst inlet temperature of 850°C before test. Reprinted from (104) with permission of Elsevier Science Publishers B.V.

OSC of CeO_2-ZrO_2. They found that both the doped samples present higher ratios of Ce^{3+}/Ce^{4+} than the pure CeO_2-ZrO_2, which leads to more crystal defects, and a much higher OSC and DOSC after a hydrothermal aging process at 1050°C. The enhanced thermal stability of CeO_2-ZrO_2 by the introduction of PrOx was confirmed by the facts that no phase segregation was measured with XRD and only a small loss of the surface area after 1050°C aging. Wang et al. (108) found that the addition of a small amount of PrOx (about 5%) to CeO_2-ZrO_2 in a Pt-Pd-Rh/CeO_2-ZrO_2 catalyst improves the light-off performance (50% conversion) of NO reduction with C_3H_6. The addition of PrOx also leads to wider operation window for NO conversion (>80%) at oxygen lean condition than that of the catalyst without PrOx. Wang et al. examined the incorporation of Pr oxide (109) and Nd oxide (110) into the CeO_2-ZrO_2 and applied the support in a Pd-only TWC. They found that the addition of appropriate amounts of Pr oxide (8 wt %) and Nd oxide (5 wt %), respectively, leads to a superior three-way performance and enlarged the operation temperature window especially for the samples aged at 1100°C for 4 h. The major reason for the promotion effect of the Pr and Nd oxides is the formation of a homogeneous ternary solid solution with higher OSC and better reducibility. Another work of Wang et al. (111) confirmed the positive effects of La, Pr, and Nd oxides addition to CeO_2-ZrO_2 on the three-way performance of the fresh and aged Pd/CeO_2-ZrO_2 catalyst.

Vidmar et al. (112) found that the addition of Y_2O_3 with an appropriate amount (5 mol %) to $Ce_{0.6}Zr_{0.4}O_2$ increases the low temperature OSC. They observed the formation of a homogeneous cubic phase in the sample. Markaryan et al. (113) also found that a small amount of Y_2O_3 addition stabilizes the cubic structure and favors the reduction of CeO_2-ZrO_2. Hu (114) used a $Ce_{0.6}Zr_{0.3}Y_{0.1}O_2$ material as the support of a Pd-only TWC and got a high light-off performance (50% conversion) for HC, CO, and NO eliminations. He

proposed that this effect is related to the excellent redox property of the Y_2O_3 modified Ce-Zr mixed oxide. Yamamoto and Tanaka (115) tested the performance of several Pd-only catalysts supported on Al_2O_3, (Ce-Zr)Ox/Al_2O_3, and (Ce-Zr-Y)Ox/Al_2O_3. They found that the best three-way performance and the 50% conversion window under air/fuel fluctuation conditions were obtained on the sample with support containing Y_2O_3, which retained a superior activity after the 1050°C vehicle emission test. They believed that the improved OSC and its stability of the Ce-Zr-Y oxide is the major reason for this high performance (116). Wang et al. (117) investigated a series of Pd-only catalyst with the composition of Pd/(Ce-Z-M)Ox/Al_2O_3 (M = Y, Ca, or Ba) calcinated at 1100°C in air for 2 h. As shown in Fig. 12, the Y_2O_3 promoted catalyst has better propane oxidation activity than the others, which suggests the Pd/(Ce-Zr-Y)Ox/Al_2O_3 catalyst is a promising CCC for high-temperature application. Moreover, this Pd/(Ce-Zr-Y)Ox/Al_2O_3 also shows the best resistance towards sulfur poisoning. Another work (118) of the same group confirmed the positive effect of Y_2O_3 on the propane combustion activity of Pd/CeO_2-ZrO_2 catalyst. XPS results indicated that an appropriate amount of Y_2O_3 addition leads to a stronger interaction between Pd species and Zr-containing species, which improves the dispersion of Pd.

The effects of Fe (119) and Ni (120) oxides incorporation into the CeO_2-ZrO_2 material and the supported Pd-only TWC were examined by Li et al. They found that the addition of both the two oxides leads to the formation of Ce-Zr-M-O ternary solid solution and more oxygen vacancy, enhancing the performance of the corresponding Pd-only TWC as a result. Another work of this group (121) found that the introduction of Fe and Ni oxides enhances the oxygen mobility of the sample. Furthermore, XPS results demonstrated that Fe and Ni oxides promote the surface atom ratios of Ce/Zr and make part of Ce^{4+} transferred into Ce^{3+}, increasing the OSC of the catalyst.

3.2.3. Promoter for Catalyst with CeO_2-ZrO_2

Modification of Pd by introduction of a promoter appears to influence the performance of Pd-based catalyst significantly. Guo et al. (122) examined the effect of La_2O_3 on the performance of a Pd/CeO_2-ZrO_2 catalyst. The results indicate that the addition of La_2O_3 to the Pd catalysts significantly enhances the light-off performance (50% conversion) after aging at 900°C for 4 h. Yao et al. (123) confirmed the positive effect of La_2O_3 on the thermal stability of a Pd/CeO_2-ZrO_2-Y_2O_3-Al_2O_3 CCC. Their results indicate that the addition of 10% La_2O_3 to the Pd catalysts significantly enhances the C_3H_8 conversion after aging at 1000°C for 5 h. They found a higher dispersion and reducibility of Pd over La_2O_3 modified catalyst than the La_2O_3 absent one. A promotional effect of NiO on the performance of Pd-NiO/CeO_2-ZrO_2/Al_2O_3 catalyst for the stoichiometric NO+CO+O_2 reaction was observed in Hungría et al. (124,125). Although no obvious change of Pd electronic properties were found by the in

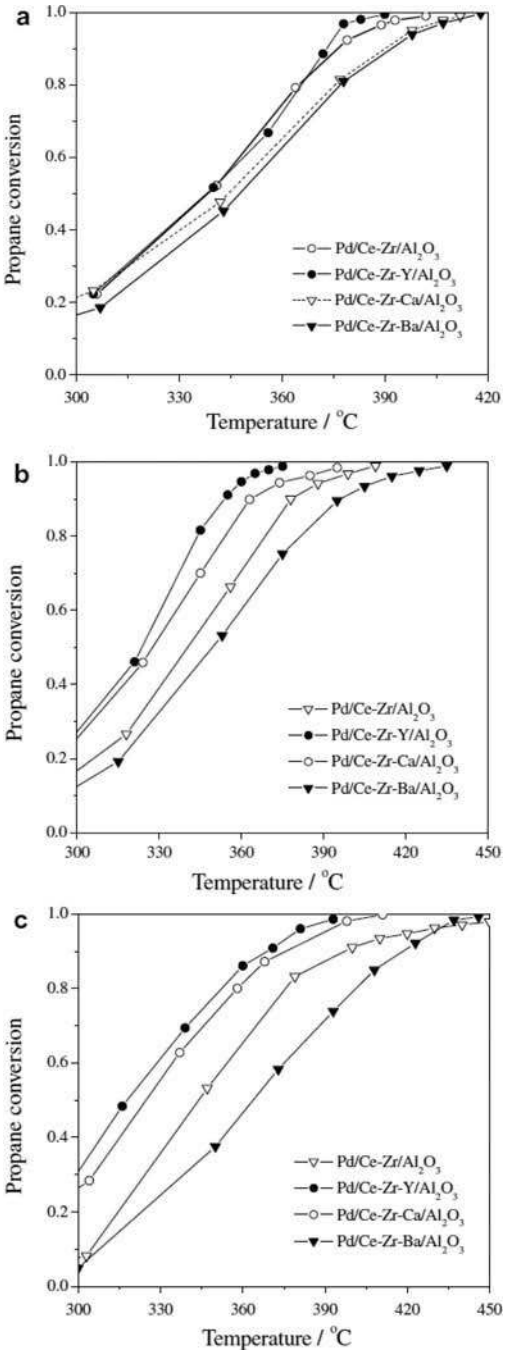

Figure 12: Propane conversion over $Pd/Ce\text{-}Zr/Al_2O_3$ and $Pd/Ce\text{-}Zr\text{-}M/\ Al_2O_3$ (M = Y, Ca or Ba) catalysts: (a) calcined at 900°C, (b) calcined at 1100°C, and (c) after sulfur-treated. Sulfur treated catalyst: After calcination at 1100°C for 2 h, the catalyst was treated under the stream containing 360 ppm SO_2, 10% O_2 and balance N_2 at 400°C for 1 h. Reprinted from (117) with permission of Elsevier Science Publishers B.V.

situ XANES characterization, the introduction of NiO leads to a preferential interaction between Pd and (Ce-Zr)Ox. The generation of more active Pd-(Ce-Zr)Ox interface enhances the CO oxidation and NO reduction activity.

Hungría et al. (126) investigated the performance of a Pd-Cu/CeO_2-ZrO_2/Al_2O_3 catalyst for the CO + NO + O_2 reaction under stoichiometric condition and found that Cu addition enhances CO oxidation and NO reduction compared to the catalyst without Cu. They believed that Cu assists to stabilize the metallic Pd due to the formation of a Pd-Cu alloy, which was confirmed by in situ XANES. The formation of Pd-Cu alloy enhances the N-O bond dissociation which is thought to be the rate-limiting step for the NO reduction reaction on the Pd-Cu/CeO_2-ZrO_2/Al_2O_3 catalyst. However, they found that the destruction of the Pd-Cu alloy happened at a high temperature (over 227°C), which removes the promoting effect of Cu for NO reduction. A DFT study (127) predicted the nature of NO interactions change from nearly covalent for the pure Pd to a mixture of covalent plus ionic for the Pd-Cu alloy. The ionic nature increases with the Cu content in the alloy and weakens the N–O bond progressively, which suggests a strong activation of NO with respect to Pd was achieved on this alloy. Iglesias-Juez et al. (128) compared the CO and NO elimination activity of Pd/CeO_2-ZrO_2 catalysts incorporated with Cr and Cu prepared with coimpregnation technique under the stoichiometric conditions of CO + NO + O_2. Their results showed that the additives have no significant influence on the CO elimination activity except in the case of Pd-Cu/CeO_2-ZrO_2 catalyst where a promoting effect was observed and mostly resulted from the presence of active species Cu (I). For NO removal, the addition of Cu and Cr both enhance the performance between 100°C and 180°C. However, poor activity with respect to Pd/CeO_2-ZrO_2 was observed on the Cu-doped one above 180°C. They believed the difference of performance on different systems may arise from the interactions between Pd and the second metals. Cr and Cu appear to form corresponding PdM alloy during the reaction. However, it is important to note that both of the two alloy species are unstable, decomposing to give a final Pd (0)-species above 177°C (PdCu) and 277°C (PdCr).

In general, the formation of Pd-M alloy strongly modifies the electronic properties of Pd, which may significantly enhance the performance of CO and NO elimination. However, the poor stability of the alloy under reaction conditions severely limits the practical value in three-way catalysis. More efforts should be made on this aspect in the future.

3.3. Catalyst Preparation

Catalysts prepared by different methods have different noble metal dispersions, metal support interactions (MSI) and therefore exhibit different catalytic performance. The technique for loading the Pd metal onto/into the support is a key factor in the preparation of the Pd-based TWCs. Normally,

almost all the Pd-based TWCs adopt impregnation method to make more Pd atoms disperse on the outer surface of the support. However, some other techniques such as deposition-precipitation (129), coprecipitation (130), sol-gel (36,99,131–133), and combustion (134,135) techniques have also been examined for the loading of Pd metal.

In general, catalysts prepared with the impregnation method have weak MSI, while the coprecipitation technique facilitates a strong MSI (SMSI). Zhou et al. (130) prepared a $LaFe_{0.77}Co_{0.17}Pd_{0.06}O_3$ catalyst with a conventional coprecipitation method and a $Pd/LaFe_{0.8}Co_{0.2}O_3$ catalyst with impregnating the $LaFe_{0.8}Co_{0.2}O_3$ support. They found that the three-way performance of the $Pd/LaFe_{0.8}Co_{0.2}O_3$ catalyst is much better than that of the $LaFe_{0.77}Co_{0.17}Pd_{0.06}O_3$ catalyst. A homogeneous distribution of Pd particles over the $Pd/LaFe_{0.8}Co_{0.2}O_3$ catalyst was observed, while no Pd particles could be found on the $LaFe_{0.77}Co_{0.17}Pd_{0.06}O_3$ catalyst by the TEM technique (Fig. 13). The H_2-TPR results showed that the reduction temperatures of Pd (II) are 85 and 240°C for $Pd/LaFe_{0.8}Co_{0.2}O_3$ and $LaFe_{0.77}Co_{0.17}Pd_{0.06}O_3$, respectively. They believed that the higher activity of the catalyst prepared by the impregnation technique is attributed to the fact that Pd is localized on the perovskite surface and easily to be reduced. However, the Pd is in the lattice of the perovskite-type oxide for the catalyst obtained with the coprecipitation technology, the SMSI occurs which decreases the reducibility of Pd in the sample.

Sol-gel technique is often used in the preparation of catalyst which has been reported to be able to prepare catalyst with a homogeneous distribution of the components (99). Kim and his co-workers (38,99) employed a sol-gel method to prepare a Pd-VOx-ZrO_2-Al_2O_3 catalyst. They synthesized this catalyst by first dissolve aluminum isopropoxide (AIP) in deionized water and then NH_4OH was added for hydrolysis and condensation. After that the Zr, V, Pd precursors in an acetone solutions were added sequentially. They postulated that the bridging V-O-Zr in tetrahedral $(M\text{-}O)_3V = O$ is responsible for the high activity and resistance against SO_2. In another work of Kim et al. (136), they examined the effect of pH (pH = 4, 10) on the behavior of a Pd/Al_2O_3 catalyst prepared by sol-gel method and found that the sample prepared at pH = 10 exhibits higher metal dispersion, larger BET surface area and better three-way performance than the other one. They believed that Pd is preferentially interacted with oxygen in alumina and forms the Pd-O-Al bond in the Pd/Al_2O_3 (pH = 10) catalyst. While no such significant interaction occurs in the catalyst of Pd/Al_2O_3 (pH = 4), and most of the Pd atoms are largely agglomerated on the external surface of Al_2O_3 in this sample. The schematic model of the Pd/Al_2O_3 catalyst prepared at different pH is shown in Fig. 14. A perovskite-type LaFePdO*x* catalyst which shows self-regenerative function and high stability, was prepared through an alkoxide method by Nishihata and his co-workers (132,133). The results showed that the Pd can reversibly

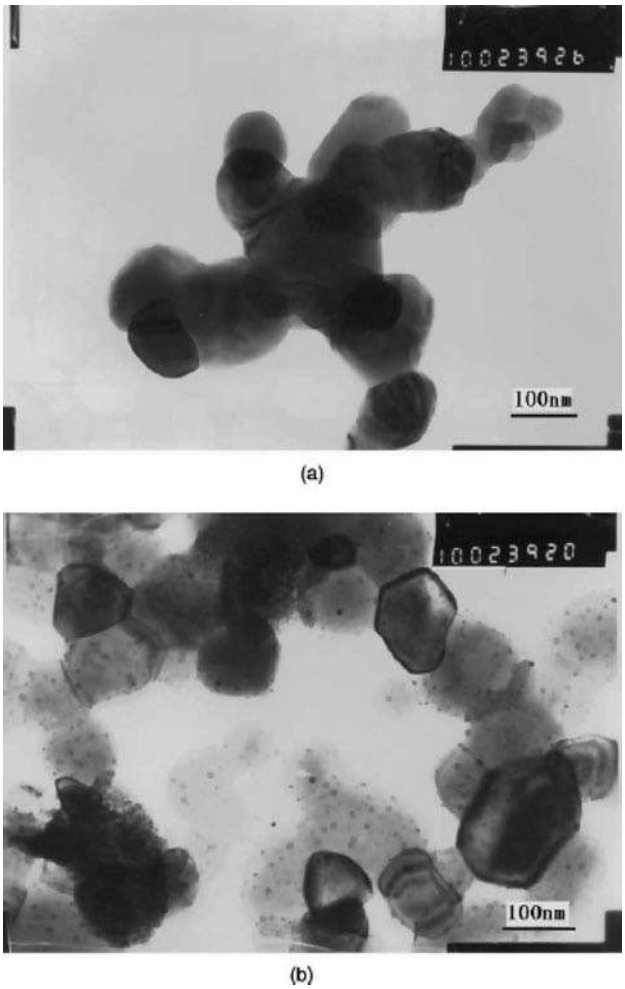

Figure 13: TEM photographs of catalysts: (a) $LaFe_{0.77}Co_{0.17}Pd_{0.06}O_3$ and (b) $Pd/LaFe_{0.8}Co_{0.2}O_3$ after activity evaluation. The activity measurements were carried out from 100 to 500°C at a rate of 5°C min^{-1} with a space velocity 45,000 h^{-1}. Reprinted from (130) with permission of Elsevier Science Publishers B.V.

move into and out of the perovskite lattice as the catalyst is cycled between the oxidative and reductive atmospheres, and this movement suppresses the growth of metallic Pd particles and maintains the high performance during the long-term aging.

Bera et al. (134) prepared a Pd/CeO_2 catalyst by using a single step solution combustion method. They mixed the precursors of $(NH_4)_2Ce(NO_3)_6$, $PdCl_2$ and $C_2H_6N_4O_2$ (oxalyldihydrazide) in the molar ration of 0.99: 0.01: 2.33 and then made it combustion in a muffle furnace. They proposed the presence of the-$O^{2-}Ce^{4+}$-$O^{2-}Pd^{2+}$-O^{2-} type of linkages on the CeO_2 surface and the lower

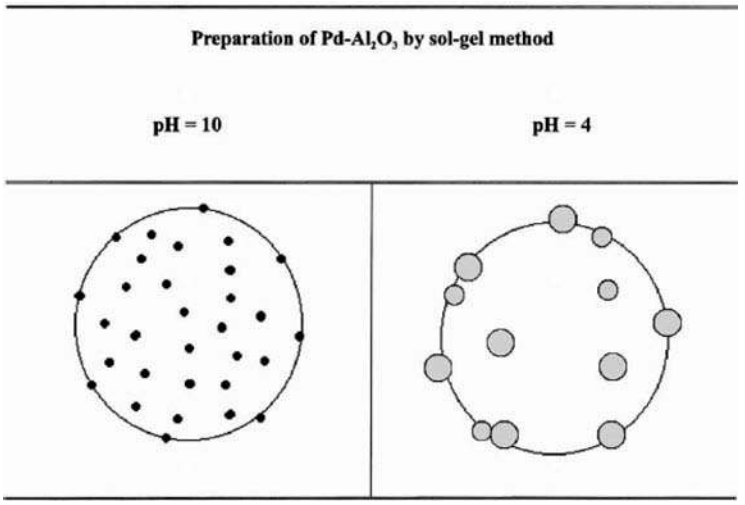

Figure 14: Schematic representations of Pd/Al_2O_3 (pH = 4) and Pd/Al_2O_3 (pH = 10) prepared by sol-gel method. For Pd/Al_2O_3 (pH = 4), Pd preferentially interacted with Al and form formation of Altetra–O–Pd bond; For Pd/Al_2O_3 (pH = 10), Pd is largely agglomerated on the external surface. Reprinted from (136) with permission of Elsevier Science Publishers B.V.

valence ionic Pd^{2+} substitution for Ce^{4+} ions can create more oxygen ion vacancies, which are beneficial for the three-way performance. Moreover, such ionically dispersed Pd/CeO_2 catalyst was confirmed to have better activity and higher selectivity for N_2 than the ionically dispersed Pt or Rh in CeO_2 ones for the reaction of NO reduction by CO.

Generally, although some other methods such as sol-gel, coprecipitation, and combustions have been investigated, the impregnation method still remains the most effective way for the production of Pd-based TWCs. The high dispersion and redox ability of Pd can be achieved by the impregnation method.

The nature of the Pd precursor salt utilized in the preparation also influences the performance of the catalyst. Monteiro et al. (137) prepared three Pd/Al_2O_3 catalysts by impregnating $PdCl_2$, $Pd(NO_3)_2$, and $Pd(acac)_2$ on γ-Al_2O_3. Higher dispersions (51%) of Pd for the catalysts prepared from $PdCl_2$ and Pd $(acac)_2$ salts than that (16%) of using $Pd(NO_3)_2$ were obtained. This phenomenon is attributed to the interactions between the hydroxyl groups on the γ-Al_2O_3 surface and the chloride, acetylacetonate anions, while the lack of such interactions lead to the lower dispersion on the catalyst prepared from $Pd(NO_3)_2$. In another work of the same group (97), higher conversion of NO and selectivity to N_2 were achieved on Pd/Al_2O_3 prepared from $PdCl_2$ than the sample from $Pd(NO_3)_2$ for the NO+CO reaction at 220°C. Zhu et al. (138) compared the influence of Pd precursors ($PdCl_2$, $Pd(NO_3)_2$, and $Pd(NH_3)_2(NO_2)_2$) on the activity of Pd/Al_2O_3 CCC. The results showed that the catalyst prepared with $Pd(NH_3)_2(NO_2)_2$ as the precursor exhibits the best thermal stability and

activity towards removing HC, CO, and NOx. This sample also has high BET surface area and Pd dispersion. It is known that the zero charge point of the support and the pH of the aqueous solution significantly affect the interaction between the support and the metal precursor. The $Pd(NH_3)_2(NO_2)_2$ aqueous solution is strongly basic (pH~12), in which the positively charged Pd ammine complex ($(Pd(NH_3)_2)^{2+}$) may exist. At this pH value, the Al_2O_3 surface is negatively charged due to its zero charge point at pH 8-9 (139). This leads to the strong electrostatic interaction during the impregnation. In addition, the Pd ammine complex may also react with the protons of the hydroxyl groups of Al_2O_3 via an ion-exchange. The strong interaction between Pd complex and support limits the remotion and sintering of Pd particles at high temperature aging.

The order of introducing Pd and the promoters during the preparation process is another key factor for getting a satisfactory catalyst. Kim et al. (140) examined the role of La_2O_3 in the Pd-only catalyst prepared by co-impregnation ($Pd\text{-}La_2O_3/Al_2O_3$) and sequential impregnation ($Pd/La_2O_3/Al_2O_3$) procedures. The $Pd\text{-}La_2O_3/Al_2O_3$ catalyst showed higher light-off performance than $Pd/La_2O_3/Al_2O_3$, and kept its superior activity in spite of the significant loss of surface area after thermal aging at 1000°C in air for 10 h. They supposed the role of La_2O_3 in the $Pd\text{-}La_2O_3/Al_2O_3$ catalyst was a promoter to improve the thermal stability of Pd through an intimate interaction between Pd and La oxide. The XPS results suggested that La oxide suppresses the interaction between PdO and Al_2O_3 during the thermal aging. However, for $Pd/La_2O_3/Al_2O_3$ catalyst, La_2O_3 preferentially interacts with the Al_2O_3 and stabilizes the support during the thermal aging. Garcia et al. (141) found that the catalyst with Pd and V co-impregnated on Al_2O_3 shows higher activity for C_3H_8 total oxidation than step-wise impregnated catalysts. Co-addition of Pd and V species leads to the increased reducibility of the V species and a relatively high amount of V^{4+} within the bulk and on the surface of the catalyst.

The preparations of both the OSC material have great impact on the physiochemical properties and performance of the Pd-only catalyst. Wang et al. (142) compared the $CeO_2\text{-}ZrO_2\text{-}Al_2O_3$ OSC material prepared with five different techniques and the performance of the corresponding supported Pd-only TWCs. The results showed that the OSC materials derived from coprecipitation with supercritical drying and microemulsion methods exhibit better textural and structural properties than those prepared from conventional co-precipitation, sol-gel, and impregnation techniques, resulting in higher three-way activity of the corresponding supported Pd-only catalyst. The difference between the $CeO_2\text{-}ZrO_2/Al_2O_3$ samples prepared by coprecipitation with supercritical drying and conventional drying method suggests that the drying process determines the properties of the Pd-only TWCs. The structural

homogeneity and thermostability of the coprecipated (CPA) and the deposition-precipitated (DPA) CeO_2-ZrO_2 aerogels were investigated in (143). After calcinated at 1000°C for 2 h in air, the CPA sample exhibited much higher surface area (39 m^2/g) than that (12 m^2/g) of the DPA one. The SEM and TEM characterization showed that the particles aggregated severely in the DPA sample while the CPA one remained relatively dispersed and separated particles with homogeneous surfaces. Furthermore, the XRD result indicates a homogeneous single-phase structure in the CPA aerogel, while in the other sample small amount of monoclinic m-ZrO_2 phase was detected. The phase separation and the low thermostability of the DPA sample may come from the weak interaction between Ce and Zr oxides due to the preparation method. Compared to the conventional coprecipitation method, the surfactant-controlled synthesis with adding a cationic surfactant during the preparation have been proved to enhance the surface area of CeO_2-ZrO_2 (144) and induce the creation of cationic defects in the CeO_2-ZrO_2 crystallite structure (145), which favors the formation of highly mobile oxygen species and promotes the surface reaction. Finally, in addition to the techniques mentioned above, it is worth mentioning some other synthetic methods have also been applied to prepare the TWCs OSC materials, e.g,. citrate complexation (50,146), hydrothermal synthesis (114,147), high-energy ball-milling (148), fusion (12), etc.

3.4. Catalyst Component Configuration

It was reported that about 80% of the total HCs produced during the Federal Test Procedure 75 (FTP 75) are emitted in the first 5 min (149). This phenomenon arises from the low catalyst bed temperature and the fuel-rich engine operation during this period. In order to eliminate the large amount of HCs emission during the cold start, many schemes have been developed to solve this problem such as CCC (45), electrically heated catalyst (150), and hydrocarbon adsorbers (151).

Among these schemes, the application of CCC represents an option for the combination of sufficiently high activity for HCs conversion, reasonable cost and minimal system complexity (152). However, the CCC is exposed to the exhaust gas with very high temperature, *ca.* 1000–1200 °C, as it locates near to the engine. As a consequence, CCC must have super stability to resist the high temperature deactivation. As shown in Fig. 15 (153), a CCC is generally followed by at least another one brick as the underfloor catalyst. The multi-brick system is an intelligent design of the process which maximizes the function and minimizes the demand of the catalysts. It has been widely accepted that the main advantage of the Pd-based catalyst over the conventional Pt-Rh catalyst is its superior activity for HC oxidation at high temperatures as well as its thermal stability (154,155).

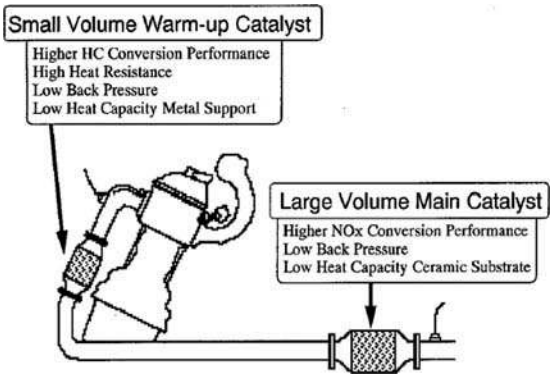

Figure 15: Typical dual TWC reactor system composed of a small-volume warm-up close-coupled catalyst and a large-volume under-floor catalyst. Reprinted from (153) with permission of Springer.

Hu et al. (45) developed a Pd-only CCC and aged it on the test vehicle for 24 h at 950 and 1050°C under the standard of FTP75. Although both the CO and NO*x* conversions decrease with the increase of the aging temperature, the HC conversion maintains almost constant even after 1050°C aging compared to the fresh catalyst. This result suggests that this Pd-only catalyst can be employed as the CCC due to its excellent thermal stability for HC removal which is the main function of the CCC. In another work of the same group (156), the influence of the small volume warm-up catalyst was examined. They designed a cascade system employing the dual-brick Pd-only catalyst with a small brick as CCC while a larger brick as the underfloor catalyst, the non-cascade system was obtained by reversing the position of the two bricks. All catalysts are pre-aged at 1050°C for 24 h. The results of FTP-75 tests showed an advantage in HC light-off performance for the cascade system, since the first small volume catalyst heats up rapidly and provides hot gases to the second catalyst once the exothermic reactions start. This suggests that a smaller brick which decrease the light-off time is preferred for the CCC application. Summers et al. (30) performed a number of experiments to investigate the impacts of the placement of the dual converters on the vehicle emission control. They compared the performance of two dual-brick Pd-only catalysts with the same overall composition but different Pd distribution, one has 2.6 g/L Pd in CCC and 10.6 g/L Pd in underfloor catalyst while the other one possesses the reverse composition in CCC and underfloor catalyst. The FTP-75 test results showed that the higher loading of Pd with 10.6 g/L in the CCC leads to the lower HC emissions, suggesting that the performance of the Pd-TWCs are not only decided by the total Pd loading amount but also related to the distribution of Pd.

As discussed in this article, there is no doubt that the presence of CeO_2 improves the performance of the TWCs under dynamic conditions. However,

the Pd-only CCCs that contain substantially no OSC material exhibit excellent HC conversion performance (157–160). For instance, Hu et al. (157,158) compared the performance of Pd-only CCC with and without OSC material in the vehicle use. They found that the catalyst containing no OSC material shows better light-off performance than that with OSC material. Williamson et al. (160) compared two dual catalysts with the formulation of Ce-free and Ce-containing Pd-only front catalyst in tandem with the same Pt/Rh rear catalyst. The vehicle FTP test results indicated the front Ce-free sample shows lower non-methane hydrocarbons emissions, while the Ce-containing sample gives improved NO*x* conversion. This phenomenon arises from the fact that the OSC material enables the oxidation of CO and HCs to proceed more efficiently under the operating conditions, which leads to the excess oxidation and overheating of the CCC (157). Moreover, the deep encapsulation of Pd by CeO_2 at high temperature may also limit the function of the metal in CCC (161).

Although multi-brick system gives high conversion of the three main pollutants simultaneously, such design requires large space for the placement of different catalyst. The layered catalyst was developed in order to optimize the function of each individual component and save place as well. The firstly successfully applied Pd-only TWCs invented by Hu et al. (157,162) from Engelhard Corporation was based on the layered configuration. They (163) found that the strong interaction between Pd and CeO_2 reduces the effectiveness of Pd in catalyzing the three-way reactions at low temperature. The high OSC only plays the important role at a high temperature enough for the mobility of the oxide ion in the bulk phase. Based on this understanding, they designed a Pd-only dual layered converter. Pd in the top layer is supported on Al_2O_3, while Pd is supported on CeO_2 and Al_2O_3 in the second layer (see Fig. 16). The layered catalyst exhibits a three-way performance between the Pd/Al_2O_3 and $Pd/CeO_2/Al_2O_3$ catalyst at a low temperature (400°C). However, this catalyst gives much better performance than the other two monolayer samples at a high temperature (600°C). This result demonstrates a synergistic effect between the two layers which have high Pd effectiveness and high OSC simultaneously. Lindner et al. (31) compared the performance of three types of Pd/Rh catalyst with the same overall composition but different placement

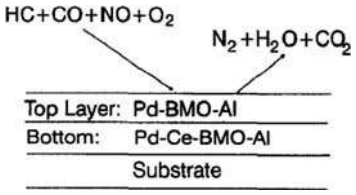

Figure 16: Schematic diagram of the layered Pd-only catalyst. Substrate is a cordierite ceramic honeycomb substrate; BMO are some base metal oxide stabilizers, details are not available in literature. Reprinted from (163) with permission of Elsevier Science Publishers B.V.

of noble metals, i.e., one single layer, two dual layers with Pd top, Rh bottom and Rh top, Pd bottom, respectively. The vehicle test results indicated the best performance was obtained on the catalyst coating Rh on the top layer and Pd on the bottom layer, while the single layer catalyst was found to exhibit the worst performance due to the formation of PdRh alloy, which suppresses the excellent catalytic activity of Rh (27). The best performance of the layered configuration (Rh top, Pd bottom) may arise from the fact that Pd is more sensitive to poisoning by contaminants from the gasoline than Pt and Rh (34). The location of Pd in the bottom layer prevents the most of the poisons and enhances the stability of the Pd component.

The layered configuration arranges the active components in a desirable environment and may induce synergy between different layers. However, some shortcomings exist which may be detrimental for the performance of the layered catalyst. The performance of a (Pd + Pt/Rh) (Pd: front, Pt/Rh: underfloor) dual-brick catalyst and a layered Pt/Rh/Pd (Pt, Rh: top layer, Pd: bottom layer) with a same overall composition was compared by Williamson et al. (157). A much better performance was found on the dual-brick catalyst configuration. The reason may be attributed to the fact that the noble metal on the bottom layer was not directly exposed to the exhaust gases, and the process that the reactant gases transfer to the surface of noble metal affects the performance of the catalyst.

The zone-coated technology which distributes the components in different layers axially along the monolith is also applied for the placement of catalyst (24). This scheme arranges the active components on different parts of the monolith brick without any interactions between them, like the serial layout of the discrete bricks. Aoki et al. (164) found that the oxygen storage characteristics depend on the ratio of CeO_2/ZrO_2. The oxygen release rate increases with the decrease of CeO_2/ZrO_2 ratio, while the optimum CeO_2/ZrO_2 ratio leads to the highest OSC. In order to effectively utilize the advantages of the OSC material, they zone-coated a material with high OSC at the front portion and a fast oxygen releasing material on the rear portion of a Pd/Rh catalyst. This catalyst was compared with a catalyst with a conventional coating which is a mixture of the same materials as those of the zone-coated one. Vehicle test results indicated that the zone coated catalyst provides a much better three-way performance than the conventional Pd/Rh catalyst.

In general, the design of catalyst component configuration helps to optimize the distribution of palladium and OSC materials, thus enhances the activity and stability of TWCs as well as lowers the loading amount of palladium. The application of Pd-CCC reduces the emission of HC to a large extent, due to the excellent thermostability and oxidation activity of Pd. However, the further control of HC should be combined with the improvements in NO*x* reduction performance of the CCC which enhances the conversion of HC, CO and NO*x* simultaneously. Layered catalyst configurations arrange

different components radially which may induce synergy between different layers, while the zone-coated technology arranges the active components on different parts of the monolith brick without any interactions between them. Currently, the layered and the zone-coated technology are usually combined in the same monolith catalyst for the optimization of the three-way performance.

4. REACTION MECHANISM AND KINETICS

In the three-way catalysis system a number of reactions happen simultaneously between different reactants (O_2, CO, NOx, CxHy, H_2, H_2O), the mechanism covering all the elementary reaction is not available. However, the mechanism and kinetics of the main reactions involved in the three-way catalysis have been investigated extensively over the past years. The overall performance of the convertor is often simulated with assuming these reactions happen at the same time.

4.1. NO Reduction Reactions

As CO is the most abundant reducing agent in gasoline powered vehicle exhaust gas, NO reduction by CO has been considered as a dominant reaction for NO removal from the automotive exhaust gas (165). A number of literatures about kinetics and mechanism of this reaction has been published. Major works have been summarized in Table 2. The overall reaction scheme of this reaction was summarized as (37):

$$NO + CO \rightarrow 1/2N_2 + CO_2 \tag{11}$$

$$2NO + CO \rightarrow N_2O + CO_2 \tag{12}$$

$$N_2O + CO \rightarrow N_2 + CO_2. \tag{13}$$

At a high temperature, reaction (11) is prevailing, while at moderate temperatures N_2O formation is favored. In the studies of the detailed mechanism of this reaction occurred on Pd catalyst, most of the researchers (166–168) adopted the Langmuir-Hinshelwood mechanism. NO and CO first compete for the adsorption on Pd surface and then the adsorbed NO species dissociate on a nearest vacant site (S). The dissociative N atom reacts with the adsorbed NO species to produce N_2O or combine to N_2, the adsorbed O will react with adsorbed CO to generate CO_2.The reaction scheme can be described as follows (166–169):

Table 2: Some reported mechanism and kinetics research results of CO+NO reaction on Pd catalyst.

References	Conditions		Mechanism and rate equations	Conclusive remarks
Muraki et al. (166)	Catalysts Pd loading Temperature Feedstock	Pd/Al_2O_3 0.006 wt % 350°C CO-NO mixture in He	$NO+S \longleftrightarrow NO_a$ $CO+S \longleftrightarrow CO_a$ $NO_a+S \rightarrow N_a+O$ $NO_a+N_a \rightarrow N_2O+2S$ $N_a+N_a \rightarrow N_2+2S$ $CO_a+O_a \rightarrow CO_2+2S$ $r_{NO} = \frac{K_1 P_{NO}}{K_2 P_{CO}}$	1. The adsorption of NO on Pd is the rate-limiting step. 2. NO reduction rate is +1 for NO and −1 for CO. 3. NO reduction rate is decided by the NO adsorption rate, CO is the inhibitor in this system.
Granger et al. (170)	Catalysts Pd loading Temperature Feedstock	Pd/Al_2O_3 1 wt% 300°C CO-NO mixture in He	$NO+S \longleftrightarrow NO_a$ $CO+S \longleftrightarrow CO_a$ $NO_a+S \rightarrow N_a+O$ $NO_a+N_a \rightarrow N_2O+2S$ $NO_a+N_a \rightarrow N_2+O_a+S$ $CO_a+O_a \rightarrow CO_2+2S$ $r_{NO} = \frac{2k3\lambda_{NO}P_{NO}}{(1+\lambda_{NO}P_{NO}+\lambda_{CO}P_{CO})^2}$	1. The formation of N_2 via adsorbed NO and N atoms is dominant. 2. The rate of NO conversion is obtained by steady-state approximation to adsorbed N atoms.
Holles et al. (167)	Catalysts Pd loading Temperature Feedstock	$Pd/CeO_2/Al_2O_3$ 4 wt% 300°C CO-NO mixture in He	The same mechanism as Muraki et al. (166) $r_{NO} = 2\left[\frac{k_4 K_1 P_{NO} N + k_5 N^2}{(1+K_1 P_{NO}+K_2 P_{CO}+N)^2}\right]$ $N = \left(\frac{-k_4 K_1 P_{NO} + \left[(k_4 K_1 P_{NO})^2 + 4k_5 k_3 K_1 P_{NO}\right]^{1/2}}{2k_5}\right)$	1. The reaction rate is obtained by steady-state approximation to adsorbed N atoms. 2. The reaction order for CO is always negative. 3. The reaction order for NO can be either positive, negative, or zero which depends on the CO partial pressure.

(*Continued*)

Table 2: (Continued).

References	Conditions		Mechanism and rate equations	Conclusive remarks
Almusaiteer and Chuang (174)	Catalysts Pd loading Temperature Feedstock	Pd/Al_2O_3 1.8 wt% – CO-NO mixture in He	Adsorption and desorption $Pd^0+NO \longleftrightarrow Pd^0\text{-}NO$ (linear) $Pd^0+CO \longleftrightarrow Pd^0\text{-}CO$ (linear) $Pd^0+NO \longleftrightarrow Pd^0\text{-}NO^-$ (bent) $2Pd^0+CO \longleftrightarrow (Pd^0)_2\text{-}CO$ (bridged) $\left(Pd^0\right)_2 - CO \xrightarrow{Pd^0 - NO} Pd^0 - CO + Pd^0$ Surface reaction $Pd^0\text{-}NO+Pd^0 \longleftrightarrow Pd^0\text{-}N+Pd^0\text{-}O$ $Pd^0+Pd^0\text{-}O \longleftrightarrow (Pd^+)_2O^{2-}$ $Pd^+ +NO \longleftrightarrow Pd\text{-}NO^+$ $Pd^0\text{-}N+Pd^0\text{-}N \longleftrightarrow 2Pd^0+N_2$ $Pd^0\text{-}NO+Pd^0\text{-}N \longleftrightarrow 2Pd^0+N_2O$ $Pd^0\text{-}CO+Pd\text{-}O \longleftrightarrow 2Pd^0+CO_2$ No rate expressions	1. The removal of adsorbed O is the rate-controlling step. 2. The process of Pd^0 oxidation to Pd^+ by NO is faster than that of the reduction of Pd^+ to Pd^0 by CO.

Mechanism 1:

$$NO + S \leftrightarrow NO_a \; K_1 \tag{14}$$

$$CO + S \leftrightarrow CO_a \; K_2 \tag{15}$$

$$NO_a + S \rightarrow N_a + O_a \; k_3 \tag{16}$$

$$NO_a + N_a \rightarrow N_2O + 2S \; k_4 \tag{17}$$

$$N_a + N_a \rightarrow N_2 + 2S \; k_5 \tag{18}$$

$$CO_a + O_a \rightarrow CO_2 + 2S \; k_6 \tag{19}$$

Muraki et al. (166) investigated the kinetics of NO reduction by CO over a Pd/Al_2O_3 catalyst at 350°C and found that the rates of CO adsorption and desorption are much more rapid than the rate of NO reduction. Hence, with assuming NO adsorption (Eq. (14)) as the rate-determining step, the reaction rate equation was obtained as:

$$r_{NO} = \frac{K_1 P_{NO}}{K_2 P_{CO}}, \tag{20}$$

where r_{NO} is the reaction rate of NO reduction, K_1 and K_2 are the equilibrium constant of NO and CO adsorption respectively, P_{NO} and P_{CO} the partial pressures of NO and CO, respectively. This equation reflects the rate of NO reduction is first order with NO and inverse first order with CO, which indicates that the rate of NO reduction is limited by NO adsorption rate and CO is a major inhibitor in this system. However, Mamede et al. (168) did not agree with the assumption in (166). They believed that the competitive adsorptions between both reactants are more in favor of NO and the rate-limiting step of this reaction should be NO dissociation, i.e., Eq. (16), while this limiting step would shift from the NO dissociation to oxygen removal process, i.e., Eq. (19), with the increase of the temperature.

Granger et al. (170) examined the kinetics of NO reduction by CO on a Pd/Al_2O_3 catalyst. The results indicates the rate constant of N_2 formation from two adsorbed N atoms (Eq. (18)) is much lower than that of N_2 generation by adsorbed NO and N atoms. They believed that Pd surface is predominantly covered by chemisorbed CO and NO molecules and the probability of combining two adjacent dissociatively adsorbed N atoms for the N_2 formation is negligible. The mechanism they adopted is similar to the mechanism 1, with exception of the replacement of the Eq. (18) by the following one:

$$NO_a + N_a \rightarrow N_2 + O_a + S \; k_7 \tag{21}$$

They applied the steady-state approximation to the adsorbed N atoms and the rate is expressed as:

$$r_{NO} = \frac{2k3\lambda_{NO}P_{NO}}{\left(1+ \lambda_{NO}P_{NO} + \lambda_{CO}P_{CO}\right)^2}. \tag{22}$$

By applying the steady-state approximation to chemisorbed O atoms, the rate of CO conversion is obtained as:

$$r_{CO} = \frac{k\lambda_{NO}P_{NO}}{\left(1+ \lambda_{NO}P_{NO} + \lambda_{CO}P_{CO}\right)^2} \tag{23}$$

$$\text{with} \quad k = k_3\left(\frac{k_4 + 2k_7}{k_4 + k_7}\right). \tag{24}$$

In these equations, k_i are the rate constants, λ_i and P_i are the fugacity coefficient and the partial pressure of component i respectively. Holles et al. (167) investigated the kinetics of CO+NO on a $Pd/CeO_2/Al_2O_3$ catalyst and found the activation energy is 76.6 kJ/mol. They believed that the different elementary reactions may be rate limiting under different conditions. Therefore, they did not assume a single rate-limiting step but employed the steady-state approximation to dissociative N atom, and the rate (based on mechanism 1) is expressed as:

$$r_{NO} = 2\left[\frac{k_4K_1P_{NO}N + k_5N^2}{\left(1 + K_1P_{NO} + K_2P_{CO} + N\right)^2}\right] \tag{25}$$

in which

$$N = \left(\frac{-k_4K_1P_{NO} + \left[\left(k_4K_1P_{NO}\right)^2 + k_5k_3K_1P_{NO}\right]^{1/2}}{2k_5}\right). \tag{26}$$

From this equation, the reaction order of CO is always negative. However, the NO reaction order can be either positive, negative, or zero. This means a high surface coverage of NO leads to a negative NO reaction order while high CO coverage results in a positive NO reaction order. This is in consistent with the trends in the reaction order plot (Fig. 17). Rainer et al. (171,172) employed the ultra-high vacuum (UHV) surface analysis technique to investigate the CO+NO reaction On Pd surface. They concluded that the removal of thermally stable N species on low-coordinated defect sites plays a role in determining

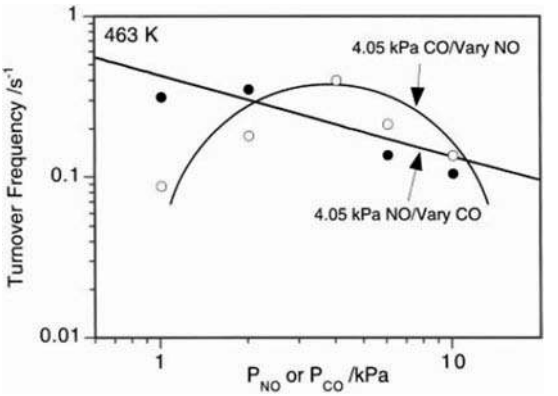

Figure 17: Turnover frequency for the NO+CO reaction on $Pd/CeO_2/Al_2O_3$ at 190°C. The closed circles are for a fixed P_{NO} = 4.05 kPa with a varying P_{CO}. The open circles are for a fixed P_{CO} = 4.05 kPa with a varying P_{NO}. Reprinted from (167) with permission of Elsevier Science Publishers B.V.

the reaction rate. The kinetic study on a 5 wt% Pd/Al_2O_3 indicated that the activation energy is 131 kJ/mol, and the reaction orders are -1 and +1.5 for CO and NO, respectively.

Almusaiteer and Chuang (173) observed that NO can chemisorb on a Pd surface as linear (Pd°-NO), bent (Pd°-NO^{-}), and cationic (Pd-NO^{+}) forms, while CO chemisorbs as linear (Pd°-CO) and bridged ((Pd°)$_2$-CO) forms. Among these forms, linear (Pd°-NO) is the active adsorbate involved in NO dissociation while linear (Pd°-CO) is active one for CO_2 formation. In another work of the same group (174), a more detailed mechanism based on in situ IR results for NO reduction by CO on a Pd/Al_2O_3 catalyst was proposed (Table 2). They observed the presence of cationic Pd-NO^{+} during the reaction at 350°C, indicating the step of Pd° oxidation to Pd^{+} by NO is faster than that of the reduction of Pd^{+} to Pd° by CO. Furthermore, the removal of adsorbed O from Pd surface to produce CO_2 was proved to be the rate-limiting step. The formation of isocyanate as Al-NCO was also detected. This species formed on Pd surface but are quickly transferred to the support surface as the following steps:

$$Pd^0 - N + Pd^0 - CO \rightarrow Pd^0 - NCO + Pd^0 \quad (27)$$

$$Pd^0 - NCO + Al \rightarrow Pd^0 + Al - NCO. \quad (28)$$

The species of isocyanate is closely related to the formation of some by-products in three-way catalysis system. Sica and Gigola (175) observed the formation of Al-NCO and found that the temperature range of the decreasing-increasing N_2O concentration is just coincident with that of the increasing-decreasing

concentration of Al-NCO species characterized by FTIR. Further, the intensity of Al-NCO bond decreases rapidly in the presence of NO above 250°C. They believed that this behavior is due to the reaction of isocyanate species with NO to produce N_2O and CO. The reaction is expressed as:

$$Al - NCO_a + NO \leftrightarrow N_2O + CO. \tag{29}$$

Newton and his co-workers (176,177) detected the formation of the intermediate PdC*x* on Pd/Al_2O_3 by high-energy X-ray diffraction (HXRD) technique during the CO/NO cycling. They found that the adsorbed CO dissociate to atomic C_a and O_a (Eq. (30)) and the active atomic C_a can diffuse to the subsurface of Pd to form PdC*x* (Eq. (31)):

$$CO_a \leftrightarrow C_a + O_a \tag{30}$$

$$Pd + C_a \leftrightarrow PdCx. \tag{31}$$

This PdC*x* phase significantly changes the adsorption form of CO, dramatically promoting the formation of linear CO species. Linear (Pd°-CO) has been proved to be more active for CO_2 formation than the bridged ((Pd°)$_2$-CO) forms (178). Moreover, PdC*x* involves in the reduction of NO, it is rapidly removed during the cycle of the NO feed (176), as:

$$PdCx + 2NO_a \leftrightarrow Pd + CO_2 + N_2. \tag{32}$$

However, the C fragments present at the Pd phase can also react with the un-dissociated NO to produce the isocyanate species bound to Pd (179,180) as:

$$PdCx + NO \leftrightarrow Pd - NCO. \tag{33}$$

Furthermore, the presence of hydrocarbons may significantly enhance the formation of NCO through this pathway, due to the supply of carbon to Pd. The formation of NCO is closely related to the formation of by-products. In addition to N_2O (175), the formation of NH_3 due to the hydrolysis of NCO was also found (181).

Despite the relatively small amount of H_2 in vehicle exhaust gas, H_2 has the potential to be applied for NO removal during the cold start engine, because the NO+H_2 reaction generally happens at substantially lower temperatures than the NO+CO reaction (182). The major works about the mechanism and kinetics of this reaction are summarized in Table 3.

Table 3: Some reported mechanisms and kinetics research results of H_2+NO reaction on Pd catalyst.

References	Conditions		Mechanism and rate equations	Conclusive remarks
Dhainaut et al. (183)	Catalysts Pd loading Temperature Feedstock	Pd/Al_2O_3 1 wt % 70°C H_2-NO mixture $NO_a+H_a \rightarrow N_a+OH_a$	$NO+S \longleftrightarrow NO_a$ $H_2+2S \longleftrightarrow 2H_a$ $NO_a+N_a \rightarrow N_2+O_a+S$ $NO_a+N_a \rightarrow N_2O+2S$ $N_a+H_a \rightarrow NH_a+S$ $NH_a+H_a \rightarrow NH_{2,a}+S$ $NH_{2,a}+H_a \rightarrow NH_3+2S$ $O_a+H_a \rightarrow OH_a+S$ $OH_a+H_a \rightarrow H_2O+2S$ $r_{NO} = \frac{2k_3\lambda_{NO}P_{NO}\sqrt{\lambda_{H2}P_{H2}}}{\left(1+\lambda_{NO}P_{NO}+\sqrt{\lambda_{H2}P_{H2}}\right)^2}$	1. The dissociation of NO is assisted by chemisorbed H atoms. 2. NO reduction rate is -0.39 for NO and +0.67 for H_2, respectively, the activation energy is 68 kJ/mol. 3. The dissociation of NO is proved to be the rate-limiting step in this system.
Dhainaut et al. (184)	Catalysts Pd loading Temperature Feedstock	$Pd/LaCoO_3$ 1 wt% 110°C H_2-NO mixture	$NO+S \longleftrightarrow NO_a$ $H_2+S \longleftrightarrow H_{2,a}$ 'O'+ $H_{2,a} \rightarrow$'V'+H_2O+S NO_a+'V' $\rightarrow$'O'+ N_a $NO_a+H_{2,a} \rightarrow NH_a+OH_a$ $NO_a+N_a \rightarrow N_2+O_a+S$ $NO_a+N_a \rightarrow N_2O+2S$ $N_a+H_{2,a} \rightarrow NH_a+H_a$ $NH_a+H_{2,a} \rightarrow NH_{2,a}+H_a$ $NH_{2,a}+H_{2,a} \rightarrow NH3+H_a+S$ $O_a+H_{2,a} \rightarrow H_2O+S$ $O_a+H_a \rightarrow OH_a+S$ $OH_a+H_a \rightarrow H_2O+2S$ 'O' is oxygen species on support; 'V': anionic vacancies from support $r_{NO} = \frac{2k_5\lambda_{NO}P_{NO}\lambda_{H2}P_{H2}}{(1+\lambda_{NO}P_{NO}+\lambda_{H2}P_{H2})^2} + \frac{2k_3k_4\lambda_{NO}P_{NO}\lambda_{H2}P_{H2}}{(k_4\lambda_{NO}P_{NO}+k_3\lambda_{H2}P_{H2})(1+\lambda_{NO}P_{NO}+\lambda_{H2}P_{H2})}$	1. The H_2 absorb on catalyst surface as molecular precursor instead of dissociative atoms. 2. NO reduction rate is -0.7 for NO and +1for H_2 respectively, the activation energy is 79 kJ/mol. 3. The reaction rate was obtained by applying the steady-state approximation to the anionic vacancies from the support 'V'.

(*Continued*)

Table 3: (Continued).

References	Conditions		Mechanism and rate equations	Conclusive remarks
Rahkamaa-Tolonen et al. (187)	Catalysts Pd loading Temperature Feedstock	Pd/Al_2O_3 1 wt% 155°C H_2-D_2-NO mixture in Ar	The mechanism of NH_3 and H_2O formation: $N_a \underset{-H_a}{\overset{+H_a}{\longleftrightarrow}} NH_a \underset{-H_a}{\overset{+H_a}{\longleftrightarrow}} NH_{2,a} \underset{-H_a}{\overset{+H_a}{\longleftrightarrow}} NH_3 + 2S$ $O_a \underset{-H_a}{\overset{+H_a}{\longleftrightarrow}} OH_a \underset{-H_a}{\overset{+H_a}{\longleftrightarrow}} H_2O + 2S$	1. Ammonia and water were formed by stepwise hydrogenation of adsorbed nitrogen and oxygen atoms. 2. The dissociation of NO is the rate-controlling step of the overall reaction.

Dhainaut et al. (183) supposed that the dissociation of NO is assisted by chemisorbed H atoms, and used a classical Langmuir-Hinshelwood mechanism to describe the NO + H_2 reaction on the Pd/Al_2O_3 catalyst:

$$NO + S \leftrightarrow NO_a \; K_1 \tag{34}$$

$$H_2 + 2S \leftrightarrow 2H_a \; K_2 \tag{35}$$

$$NO_a + H_a \rightarrow N_a + OH_a \; k_3 \tag{36}$$

$$NO_a + N_a \rightarrow N_2 + O_a + S \; k_4 \tag{37}$$

$$NO_a + N_a \rightarrow N_2O + 2S \; k_5 \tag{38}$$

$$N_a + H_a \rightarrow NH_a + S \; k_6 \tag{39}$$

$$NH_a + H_a \rightarrow NH_{2,a} + S \tag{40}$$

$$NH_{2,a} + H_a \rightarrow NH_3 + 2\,S \tag{41}$$

$$O_a + H_a \rightarrow OH_a + S \tag{42}$$

$$OH_a + H_a \rightarrow H_2O + 2\,S \tag{43}$$

Kinetics results indicated $(k_4 + k_5)\,\lambda_{NO}P_{NO} \gg k_6\lambda_{H2}P_{H2}$, and the rate equation was obtained as:

$$r_{NO} = \frac{2k_3\lambda_{NO}P_{NO}\sqrt{\lambda_{H2}P_{H2}}}{\left(1 + \lambda_{NO}P_{NO} + \sqrt{\lambda_{H2}P_{H2}}\right)^2} \tag{44}$$

where k_3 is the rate constant of Eq. (36), in which NO dissociation is assisted by chemisorbed H atoms, P_{NO} the partial pressure of NO and P_{H2} the partial pressure of H_2, λ_{NO} fugacity coefficient of NO and λ_{H2} fugacity coefficient of H_2. This rate expression suggests that the dissociation of NO is the rate-limiting step in this system. In another work, Dhainaut et al. (184) examined the kinetics of the NO + H_2 reaction on a $Pd/LaCoO_3$ catalyst and found that the reaction orders with respect to the partial pressure of H_2 and NO were 1 and -0.7 respectively. They believed NO may strongly adsorb on catalyst surface where the probability of finding two adjacent sites for the dissociative adsorption of hydrogen would be very low. Therefore, H_2 should remain adsorbed as a precursor of molecular species on the $Pd/LaCoO_3$ catalyst. A bi-functional mechanism involving anionic vacancies at the support of was proposed.

The main drawback of the NO+H_2 reaction over Pd is the low selectivity of N_2, especially at low temperatures (185,186). A more than 70% N_2O selectivity was observed over Pd catalyst at 120°C for NO+H_2 reaction, but it quickly decreases with the increase of the temperature (185). The partial reduction of NO by H_2 is the dominant reaction at low-temperatures as:

$$2NO + H_2 \rightarrow N_2O + H_2O \tag{45}$$

Chambers et al. (186) compared the CO+NO and NO+H_2 reaction over Pd/SiO_2 catalyst. As shown in Fig. 18, N_2O is the main products for NO+H_2

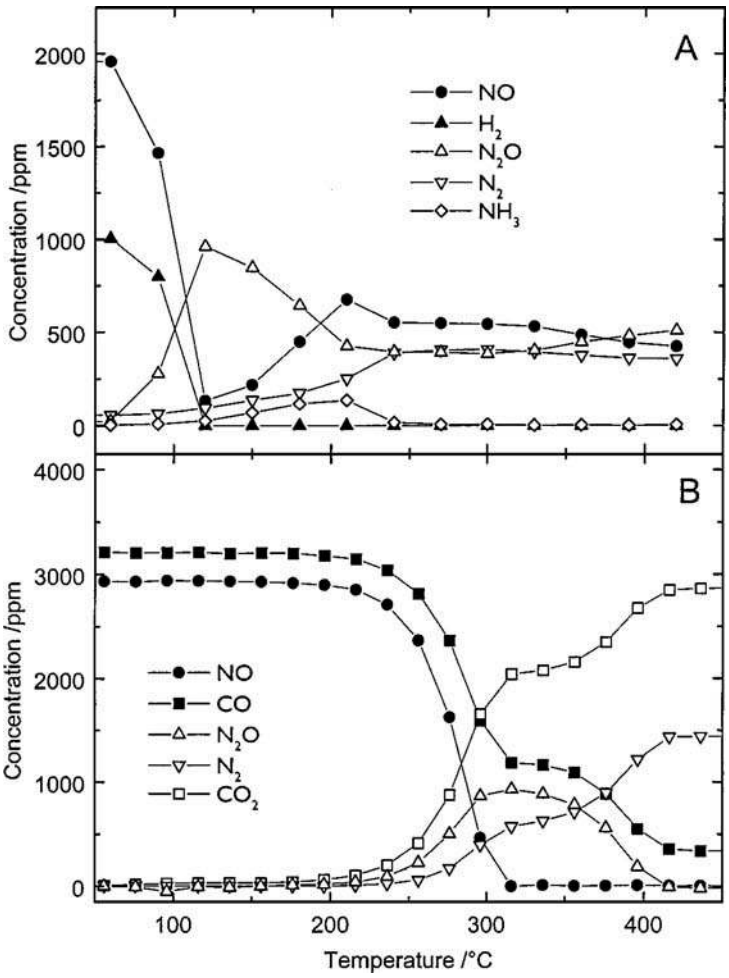

Figure 18: Reactants and products concentrations as a function of temperature for the binary reactions over 75 mg Pd/SiO_2. (A) 2000 ppm NO+1000 ppm H_2+N_2 balance. (B) 2900 ppm NO+3450 ppm CO+N_2 balance. Reprinted from (186) with permission of Elsevier Science Publishers B.V.

reaction below 200°C, while N_2O was found above 250°C for NO+CO reaction. Moreover, the formation of NH_3 was also observed between 150–225°C during NO+H_2 reaction. Rahkamaa-Tolonen et al. (187) explored the mechanism of NH_3 formation in NO+H_2 reaction over a Pd/Al_2O_3 by a hydrogen-deuterium exchange experiment. The isotopic transient experiments confirmed that ammonia and water are produced by stepwise hydrogenation of adsorbed N atoms and O atoms respectively (see Table 3), which had been adopted also by Dhainaut et al. (183,184). Recently, Oh and Triplett (188) investigated the formation of NH_3 over Pd/Al_2O_3 catalyst under a simulated gas containing 0.45% H_2, 1500 ppm NO, 1.8% CO, 1000 ppm C_3H_6, 0.9% O_2, 10% CO_2 and 10% H_2O. They found that NO will preferentially reacts with H_2 in the simulated gas to produce almost 100% selectivity to NH_3 between 400 and 500°C. A reaction pathway involving the CO with the overall stoichiometry was proposed:

$$NO + CO + 1.5H_2 \rightarrow NH_3 + CO_2 \tag{46}$$

The role of CO is to produce hydrogen through WGS reaction at high temperatures (above 400°C). The addition of CeO_2 and Rh to the Pd/Al_2O_3 significantly inhibits the formation of NH_3.

4.2. Oxidation Reactions

4.2.1. CO Oxidation

CO oxidation by O_2 is among the major reactions in the three-way catalysis. The major works about the mechanism and kinetics of CO + O_2 reaction have been involved in Table 4. Generally, Langmuir-Hinshelwood mechanism was adopted for this reaction over the Pd-based catalyst.

Schwab and Gossner (189) supposed that the reaction of CO + O_2 on Pd catalyst follows Langmuir-Hinshelwood type mechanism, and used the following mechanism to describe this reaction:

$$O_2 + S \leftrightarrow O_{2,a}\ Ko \tag{47}$$

$$CO + S \leftrightarrow CO_a\ K_{CO} \tag{48}$$

$$O_{2,a} + CO_a \rightarrow CO_2 + O_a\ k_3 \tag{49}$$

with assuming the surface reaction between chemisorbed carbon monoxide and chemisorbed molecular oxygen as the rate-limiting step, the rate equation was obtained as:

$$r = \frac{k_3 K_O}{K_{CO}} \frac{P_{O2}}{P_{CO}}.$$

Table 4: Some reported mechanism and kinetics research results of $CO+O_2$ reaction on Pd catalyst.

References	Conditions		Mechanism and rate equations	Conclusive remarks
Schwab and Gossner (189)	Catalysts Pd loading Temperature Feedstock	Pd – 250–320°C $CO+O_2$	$O_2+S \longleftrightarrow O_{2,a}$ $CO+S \longleftrightarrow CO_a$ $O_{2,a}+CO_a \rightarrow CO_2+O_a$ k_3 $r = \frac{k_3 K_O}{K_{CO}} \frac{P_{O2}}{P_{CO}}$	1. The surface reaction between adsorbed CO and O is the rate-limiting step. 2. CO_2 formation rate is +1 for O_2 and -1 for CO. 3. The activation energy is 93 kJ/mol
Engel and Ertl (190)	Catalysts Pd loading Temperature Feedstock	Pd (111) – 250°C $CO+O_2$	$CO+S \rightarrow CO_a$ k_1 $CO_a \rightarrow CO+S$ k_2 $O_2+S \rightarrow 2O_a$ k_3 $O_{2,a}+CO_a \rightarrow CO_2+O_a$ k_4	1. This reaction follows the Langmuir-Hinshelwood mechanism. 2. The activation energy is 105 kJ/mol at low CO coverage, while it turns to be 59 kJ/mol at moderate CO coverage.
Xu and Goodman (192)	Catalysts Pd loading Temperature Feedstock	Pd/SiO_2 – 77–727°C $CO+O_2$	The same mechanism as Engel and Ertl (190) $r = \frac{k_2 k_3 P_{O2}}{k_2+k_1 P_{CO}-k_3}(1 - \frac{k_2 k_3}{k_{4\alpha}})$ $\alpha = k_1 \frac{P_{CO}}{P_{O2}} - k_3$	1. The reaction orders with respect to the CO and O_2 pressure changes with the change of conditions. 2. The difference in the adsorption rates of CO and O_2 was involved in rate expression, which adequately describes the kinetic behavior under different conditions.

Rajasree et al. (196)	Catalysts Pd loading Temperature Feedstock	Pd/CeO_2-ZrO_2 2 wt% 300°C $CO+O_2+H_2O+CO_2+He$	$CO+S \longleftrightarrow CO_a$ $O_2+S \rightarrow O_{2,a}$ $O_{2,a}+S \rightarrow 2O_a$ $H_2O+S \longleftrightarrow H_2O_a$ $H_2O_a+O_a \longleftrightarrow 2OH_a$ $CO_a+OH_a \rightarrow CO_2+H_a+S$ $2H_a+O_a \rightarrow H_2O_a+2S$	1. The presence of H_2O significantly increases the reaction rate due to the enhancement of the bulk diffusion of oxygen in CeO_2 2. CO_2 inhibits the reaction due to the reducing of oxygen storage sites.
Kotareva et al. (197)	Catalysts Pd loading Temperature Feedstock	$PdCl_2$-$CuCl_2/Al_2O_3$ 0.4 wt% 27°C $CO+O_2+H_2O+N_2$	$CO+S \longleftrightarrow CO_a$ $CO_a+H_2O_a \longleftrightarrow (H_2O)(CO)_a$ $(H_2O)(CO)_a+O_2 \longleftrightarrow (H_2O)(CO)(O_2)_a$ $(H_2O)(CO)(O_2)_a \rightarrow CO_2+O(H_2O)_a$ $O(H_2O)_a+CO \rightarrow CO_2+H_2O+S$ $r = \frac{K_1 P_{CO} P_{O2} P_{H2O}}{(1 + K_2 P_{CO} + K_3 P_{CO} P_{H2O} + k_4 P_{CO} P_{O2} P_{H2O})}$	1. Both H_2O and O_2 may involve in the formation of CO_2 2. The presence of H_2O strongly enhances the reaction rate.

This expression indicates the reaction orders are -1 and +1 for CO and O_2, respectively. Furthermore, the activation energy obtained on this catalyst is 93 kJ/mol. Engel and Ertl (190) confirmed that the CO oxidation proceeds between two adsorbed species (Langmuir-Hinshelwood mechanism) on Pd (111) with the aid of a molecular beam technique, and no evidence for Eley-Rideal mechanism was found. However, they cannot give a simple reaction rate expression due to the changes of adsorption rates for O_2 and CO with the change of the temperature and pressure. Different from the work of Schwab and Gossner (189), Szanyi et al. (191) evaluated the kinetics of CO oxidation reaction on Pd (111) and suggested that the step of CO desorption is rate-controlling due to the predominantly coverage of Pd surface by CO. Moreover, the reaction between adsorbed CO and adsorbed O is very fast and CO_2 desorbs rapidly upon formation. Xu and Goodman (192) investigated the kinetics of CO + O_2 on Pd/SiO_2 over the wide range of pressure from 10^{-9} to 15 Torr and temperature from 77 to 727°C. They found that the CO oxidation rate increases with the surface temperature to a maximum and then gradually declines. Likewise, the reaction orders for CO and O_2 vary with the reaction temperature as well. This change in kinetic behavior arises from the change in the rate-limiting step with reaction conditions. With applying a similar mechanism, Schwab and Gossner (189) proposed a generic rate equation (see Table 4) which contains the difference in the adsorption rates of CO and O_2. This equation fits well with the kinetic data of CO oxidation over the conditions examined.

Recently, Balmes et al. (193) observed that a PdC*x* phase forms and disappears reversibly in the CO/O_2 mixture. This result strongly indicates that the dissociation of CO is involved in the CO oxidation over Pd catalysts as:

$$CO_a \leftrightarrow C_a + O_a \tag{50}$$

$$Pd + C_a \leftrightarrow PdCx \tag{51}$$

$$PdCx + 2O_a \rightarrow Pd + CO_2 \tag{52}$$

The CO oxidation activity over Pd catalysts are enhanced by the presence of hydroxyls groups on the surface of Pd catalyst. The interaction between CO and hydroxyls groups lead to the formation of carbonate or formate species as precursors which favors the breaking of C-O bond (194,195).

Rajasree et al. (196) looked at the effects of CO_2 and H_2O on the transient kinetics of CO oxidation over a Pd/CeO_2-ZrO_2 catalyst. Their results showed the presence of H_2O significantly increases the reaction rate due to the enhancement of the bulk diffusion of oxygen in CeO_2, while CO_2 inhibits the reaction owing to the reducing of oxygen storage sites. Kotareva et al. (197)

confirmed the positive effect of H_2O on the rate of CO_2 formation on a $PdCl_2$-$CuCl_2/Al_2O_3$. The reaction order with respect to H_2O was obtained as +0.6.

4.2.2. *Propane and Propene Oxidation*

The elementary step reactions for propylene/propane oxidation (containing hundreds of elementary steps) (198) are very complex and not available in this article. Based on the collision theory, a simplified mechanism was proposed as (199):

$$P + S \leftrightarrow P_a \tag{53}$$

$$P_a + S \leftrightarrow P_{1,a} + R_a \tag{54}$$

$$P_{1,a} + S \leftrightarrow 2R_a \tag{55}$$

$$R_a + 3O_a \leftrightarrow CO_2 + H_2O_a + 2S \tag{56}$$

where $P_{1,a}$ and R_a denote the cracking products containing two and one carbon atoms, respectively. The R_a finally reacts with the adsorbed oxygen to produce H_2O and CO_2. CO_2 appears to have no influence on propane and propene oxidation, due to the rapidly and completely desorption from the catalyst surface (200,201). However, the presence of an excess of water vapor causes the deactivation of the catalyst, attributed to the formation of palladium hydroxide (201). The slow step of this reaction has been proposed as the dissociative adsorption of propene and propane (202).

The kinetics result of propene and propane combustion over Pd-based catalyst was summarized in Table 5 (33,200–203). Yao (33) investigated the kinetics of Pd-based catalyst under the oxygen-rich conditions and found that the reaction orders of C_3H_6 are -0.6 and -0.7 for Pd wire and Pd/Al_2O_3,

Table 5: Kinetics of propene and propane combustion over Pd-based catalyst.

Reference	Reactant	Catalyst	Reaction order			Activation energy (kJ/mol)
			C_3H_x	O_2	H_2O	
Yao (33)	C_3H_6	Pd wire	−0.6	1.5	–	126
Yao (33)	C_3H_6	Pd/Al_2O_3	−0.7	1.0	–	92
Yao (33)	C_3H_6	$Pd/CeO_2/Al_2O_3$	0.4	0.2	–	54
Yao (202)	C_3H_8	Pd wire	0.4	0	–	109
Yao (202)	C_3H_8	Pd/Al_2O_3	0.6	0.1	–	63
Aryafar and Zaera (203)	C_3H_8	Pd foil	1.0±0.1	0.0±0.2	–	56
van de Beld (200)	C_3H_8	Pd/Al_2O_3	0.61	−0.46	0	119
Cullis and Nevell (201)	C_3H_8	Pd/Al_2O_3	1.0±0.1	–	–	65

respectively. However, the reaction order of C_3H_6 changes to +0.4 for a $Pd/CeO_2/Al_2O_3$ catalyst, suggesting the inhibiting effect of propene was retarded by CeO_2 addition. In another work of Yao (202), the kinetics of C_3H_8 oxidation was investigated. They found that the reaction order of C_3H_8 is positive for all the Pd-based catalysts. This result is supported by the other works in Table 5, as the reaction rates show positive dependence on the propane partial pressure. The difference of combustion kinetics between propene and propane over Pd catalysts was due to the stronger adsorption of propene over palladium (102).

5. CATALYST DEACTIVATION

According to the previous research works, the phenomenon of deactivation for Pd-based TWCs may have different origins, e.g., thermal and chemical deactivations (3,35,71,204–207).

Sintering of the noble metals and the OSC materials in the catalyst, leading to the loss of active surface area and OSC, represent the most important factors for the deactivation of the TWCs (9). In the work of Iglesias-Juez et al. (204), the apparent drop of the Pd-only catalyst activity after 1000°C aging for 12 h was interpreted as a consequence of the significant Pd sintering. It was also reported that the light-off performance of the Pd-only CCC improves with the increased Pd dispersion (160), suggesting the severe sintering of Pd may deactivate this catalyst.

The sintering of the nanoparticle can be divided into two mechanism, as particle migration and coalescence or Ostwald ripening mechanism. The growth kinetics has been considered as an effective way to explore the mechanism of sintering (208). Wynblatt and Gjostein (209) proposed a growth equation for the sintering of supported catalyst as:

$$d^n - d_0{}^n = kt, \tag{57}$$

where d is the average diameter at time t, d_0 is the initial diameter for fresh catalyst, n is the growth order, and k is a constant at a given temperature. The low value (below 4) of growth order n has been considered for the particle growth by Ostwald ripening mechanism, while the high value is for particle migration and coalescence. In order to correlate the drop kinetics of dispersion with time, another form of Eq. (57) based on the change of particle dispersion has been proposed as (210)

$$D = \left(\frac{1}{D_0^n} + bt\right)^{-1/n}. \tag{58}$$

In which D is the catalyst dispersion. Xu et al. (205) examined the sintering mechanism of Pd in Pd/Al_2O_3 catalysts under accelerated aging conditions (10% H_2O, 900°C for 200 h). They found that the growth order n are both approximately 2 calculated from Eqs. (57) and (58), confirming the homogeneity of the growth order between the two equations. The Ostwald ripening mechanism which is limited by vapor phase transport is the main reason for the sintering of this Pd/Al_2O_3 catalyst. Furthermore, no equilibrium particle size or dispersion was observed within the 200 h aging. Recently, Kang et al. (211) investigated the sintering kinetics of Pd-only catalyst by the field aging with different mileage. They proposed a sintering equation as:

$$a = 1/(1 + k_d M), \tag{59}$$

where $a = D/D_0$, D is the Pd dispersion at the aging mileage M, k_d is sintering constant. As shown in Fig. 19, this model well describes the decrease of the catalyst dispersion regardless of the Pd loading content. With assuming the aging mileage and aging time to be linearly related, we obtain the growth order n of Eq. (59) as 1, suggesting a more severe Pd sintering kinetics than that in (205). Moreover, this result strongly indicates that the Ostwald ripening mechanism controlled by vapor phase transport dominates the sintering process of the Pd-only TWC under the real working conditions, even for the catalyst aging for 98,000 miles. In addition, as mentioned above, the state of Pd is strongly influenced by the particle size, and the change of Pd state from

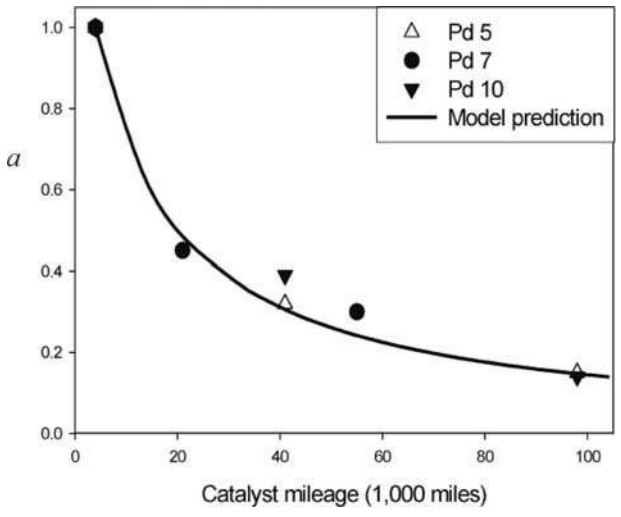

Figure 19: The drop of dispersion with respect to the catalyst mileage over Pd-only catalyst with different Pd loading. Pd5, Pd7, and Pd10 are the Pd loading ranges from 5–10 g/L. Reprinted from (211) with permission of American Chemical Society.

Pd (I) to Pd (0) during the sintering process of the catalyst also contributes to the deactivation of Pd-only TWCs.

Since the vapor pressure of PdO is lower than that of Pd metal, the aging atmosphere which may influence PdO decomposition temperature affects the sintering of Pd (212). Kang et al. (213) investigated the thermotability of Pd catalyst under oxidizing (3, 8, and 21% O_2) or reducing (3% CO) conditions with background gases containing 10% H_2O, 10% CO_2 and N_2 balance at 600 and 900°C for 16 h. They found that the catalysts aging under oxidizing conditions show better performance than that under reducing conditions. Moreover, the performance of the catalysts aged under oxidizing conditions increase with the increase of the oxygen content. The TGA results demonstrate that the higher oxygen partial pressure leads to more stable PdO. The low volatility of PdO inhibits the sintering of Pd through Ostwald ripening mechanism. McCarty et al. (210) examined the Pd sintering kinetics under the conditions of 14 vol % O_2, 10 vol % H_2O, 4 vol % CO_2, 0.5 ppmv SO_2, and the balance N_2 at 900°C. They obtained a growth order n as 3, which suggests a lower Pd sintering rate than that in (205). We believe that this lower sintering rate may arise from the oxidizing conditions which leads to the formation of PdO during the aging process.

As mentioned above, the interaction between Pd and OSC material leads to a synergetic effect which enhances the performance of catalyst. Therefore, the loss of metal-support interface during the thermal aging also contributes to the deactivation of the Pd-based TWCs (71). After aging at 1000°C for 16 h, the lower CO oxidation and NO reduction activities on a Pd/CeO_2-ZrO_2/Al_2O_3 catalyst were observed by Martínez-Arias et al. (214). In situ DRIFTS results indicated that the intensity of Pd^{2+}-carbonyl species are considerably weaker for the aged systems. This species is related to the Pd in contact with CeO_2-ZrO_2 mixed oxides, which are very active for CO oxidation and NO reduction. They proposed that the worse performance of the aged catalyst was not only due to the sintering of Pd and CeO_2-ZrO_2 but also to a consequent loss of the Pd-(CeO_2-ZrO_2) interface. Heo et al. (215) tested the performance of a filed-aged Pd-only catalyst with different mileages and found that the sintering of Pd is responsible for the initial deactivation of the catalyst, while the sintering of the CeO_2-ZrO_2 mixed oxide and the weakening of the Pd-(CeO_2-ZrO_2) interaction both contributed to the gradual decrease of the OSC and the deactivation of the TWC.

The exposure of the TWCs to the chemical additives in gasoline and the lubricating oils, such as P and S irreversibly changes the catalyst structure and causes deactivation (206). The Quantitative analyses of the poisons in an 82000 km aged Pd-only catalyst indicated that P was the main poison at the front zone of the catalyst (154). The poisoning effect arises from the incorporation of P within the subsurface of CeO_2 or CeO_2-ZrO_2 mixed oxide and produces $CePO_4$ which is very difficult to get re-oxidized, locking the Ce^{3+}/Ce^{4+} redox

couple and decreasing the OSC as a result (215,216). Moreover, Raman characterization demonstrated that the Pd-only catalyst has stronger $CePO_4$ peaks after high temperature aging, which indicates P poisoning is a high temperature mode of catalyst deactivation (217). Christou et al. (218) found that the incorporation of P causes a significant decrease of OSC for the CeO_2-ZrO_2 material. In addition to locking the Ce^{3+}/Ce^{4+} redox couple, $CePO_4$ also physically covers catalyst particles resulting in loss of BET surface area, pore volumes and active Pd sites. However, the presence of Pd on the surface of CeO_2-ZrO_2 was found to reduce the deactivating effect of P to a great extent, due to the back-spillover of oxygen from CeO_2-ZrO_2 to the oxygen vacant sites of Pd.

Beck and Sommers (155) observed the deterioration of a commercial dual brick (Pd: front, Pt/Rh: rear) catalyst due to SO_2 in the feed stream. However, this S poisoning is totally reversible after operation at 700°C which suggests that the S poisoning is more effective at low temperature. Hilaire et al. (219) compared the effect of SO_2 on the CO oxidation activity of Pd/Al_2O_3 and $Pd/CeO_2/Al_2O_3$ catalysts. The results showed that the unpoisoned $Pd/CeO_2/Al_2O_3$ catalyst has much higher activity than the unpoisoned Pd/Al_2O_3 catalyst. No light-off performance difference was observed between the SO_2 poisoned Pd/Al_2O_3 catalyst and the unpoisoned one, while a lower activity was observed with the poisoned $Pd/CeO_2/Al_2O_3$ sample compared to the unpoisoned one. This phenomenon suggests that the SO_2 poisoning in Pd-TWC primarily arises from the interaction with OSC materials. Boaro et al. (220) examined the OSC behavior of CeO_2 and CeO_2-ZrO_2 in the presence of SO_2 and found that the OSC is detrimentally affected due to the formation of $Ce_2(SO_4)_3$. The addition of ZrO_2 improves the reduction of sulfates to H_2S and increases the resistance of CeO_2 to SO_2 poisoning.

Furthermore, it is necessary to point out that the poison tends to accumulate at different part of the reactor for monolith formulation. Härkönen et al. (154) examined the distribution of poisons over an 82,000 km aged Pd-based monolith catalysts and found that the P was main poison at the front part of reactor while the S was the most abundant poison at the middle and rear position. Heo et al. (215) observed a similar poisons distribution with P deposition mainly near the inlet and S poison accumulation over the entire Pd-based monolith. In most of the cases, the catalyst deactivation does not occur for one single reason in vehicle use, but for a combination of the thermal and chemical effects.

6. CONCLUSIONS AND PERSPECTIVES

Application of Pd in TWCs represents a major breakthrough of automotive exhaust gas treatment technology. This application is crucial for lowering the

cost and enhancing the HC removal efficiency especially from the cold-start of engines. Much research on Pd-based catalyst has been made during the past several decades and the results showed that Pd has several advantages as the substitute for Pt and Rh. The Pd-only TWCs which can meet the stringent Californian low emission vehicle standards were also introduced in the 1990s. However, the intrinsically unbalanced capacity for conversion of different pollutants, relative high loading amount and fuel quality (S and P levels) still limit the application of the Pd-only TWCs in vehicle use. Currently, TWC formulations, i.e., Pd-only, Pd/Rh, Pt/Rh, and Pt/Pd/Rh are all in commercial application. It is hard to find only one formulation for all the vehicle exhaust conditions. The different formulations could be coated on different bricks, be deployed in different layers on the same brick or different parts of the same brick. The regulation standards, fuel quality, different types of exhaust composition and economic factors all affect the choice of the catalyst formulation. In general, Pd-only and Pd/Rh formulations are employed as CCC for reducing cold-start emissions, while the Rh-containing catalysts are usually used for the under-floor catalyst. For the further use of Pd in TWCs, several challenges remain to be solved.

1. Many mechanisms and kinetics of the individual reactions such as NO reduction by CO or H_2, CO and HCs oxidation over Pd catalyst have been proposed. However, the coupling effects of the third reactant, such as the influence of NO on CO oxidation reaction, or the influence of O_2 on NO reduction reaction, on the detailed mechanism and kinetics is still unclear in three-way catalysis system.
2. In order to meet the regulations for HC emissions on super low emission vehicles, efforts should be made on the development of Pd-based CCCs with ultra-high thermal stability. As the Ostwald mechanism plays a dominant role in the sintering of Pd-only catalyst under real conditions, the ultra-stable washcoat which could block the edge and corner sites of catalyst is needed. Phosphorus-modified Al_2O_3 may be a promising choice.
3. As $NO+H_2$ reaction generally happens prior to the other main reactions in three-way catalysis, this reaction is crucial for further removal of NOx in cold-start period. However, the low selectivity to N_2 over Pd-only catalyst at low temperature remains a key problem. The further investigation focus on the enhancement of low-temperature N_2 selectivity for $NO+H_2$ reaction under dynamic three-way conditions is still called for.
4. In order to further reduce the emissions of the gasoline powered engines, the concept of a four-way catalyst (FWC), which removes particulate matter (PM) in addition to the three way reactions, has been proposed.

REFERENCES

[1] Twigg, M.V.; Progress and future challenges in controlling automotive exhaust gas emissions, *Appl. Catal. B: Environ*. **2007**, *70*, 2–15.

[2] Heck, R.M.; Farrauto, R.J.; Automobile exhaust catalysts, *Appl. Catal. A: Gen*. **2001**, *221*, 443–457.

[3] Summers, J.C.; Hegedus, L.L.; Effects of platinum and palladium impregnation on the performance and durability of automobile exhaust oxidizing catalysts, *J. Catal*. **1978**, *51*, 185–192.

[4] Papavasiliou, A.; Tsetsekou, A.; Matsouka, V.; Konsolakis, M.; Yentekakis, I.V.; Boukos, N.; Development of a Ce-Zr-La modified Pt/γ-Al_2O_3 TWCs' washcoat: Effect of synthesis procedure on catalytic behaviour and thermal durability, *Appl. Catal. B: Environ*. **2009**, *90*, 162–174.

[5] Gandhi, H.S.; Piken, A.G.; Shelef, M.; Delosh, R.G.; Laboratory evaluation of three-way catalysts. SAE Paper 760201, 1976.

[6] Twigg, M.V.; Automotive exhaust emissions control, *Platinum Metals Rev*. **2003**, *47*, 157–162.

[7] Shim, W.G.; Jung, S.C.; Seo, S.G.; Kim, S.C.; Evaluation of regeneration of spent three-way catalysts for catalytic oxidation of aromatic hydrocarbons, *Catal. Today* **2011**, *164*, 500–506.

[8] Lucena, P.; Vadillo, J.M.; Laserna, J.J.; Mapping of platinum group metals in automotive exhaust three-way catalysts using laser-induced breakdown spectrometry, *Anal. Chem*. **1999**, *71*, 4385–4391.

[9] Kašpar, J.; Fornasiero, P.; Hickey, N.; Automotive catalytic converters: current status and some perspectives, *Catal. Today* **2003**, *77*, 419–449.

[10] Wang, J.; Shen, M.; Wang, J.; Wang, W.; Steam effects over $Pd/Ce_{0.67}Zr_{0.33}O_2$ three-way catalyst, *J. Rare Earth* **2011**, *29*, 217–224.

[11] Han, Z.; Wang, J.; Yan, H.; Shen, M.; Wang, J.; Wang, W.; Yang, M.; Performance of dynamic oxygen storage capacity, water-gas shift and steam reforming reactions over Pd-only three-way catalysts, *Catal. Today* **2010**, *158*, 481–489.

[12] Rao, G.R.; Fornasiero, P.; Di Monte, R.; Kašpar, J.; Vlaic, G.; Balducci, G.; Meriani, S.; Gubitosa, G.; Cremona, A.; Graziani, M.; Reduction of no over partially reduced metal-loaded CeO_2-ZrO_2 solid solutions, *J. Catal*. **1996**, *162*, 1–9.

[13] Ozawa, M.; Role of cerium-zirconium mixed oxides as catalysts for car pollution: A short review, *J. Alloy. Comp*. **1998**, *275–277*, 886–890.

[14] Ozawa, M.; Matuda, K.; Suzuki, S.; Microstructure and oxygen release properties of catalytic alumina-supported CeO_2-ZrO_2 powders, *J. Alloy. Compd*. **2000**, *303–304*, 56–59.

[15] Voltz, S.E.; Morgan, C.R.; Liederman, D.; Jacob, S.M.; Kinetic study of carbon monoxide and propylene oxidation on platinum catalysts, *Ind. Eng. Chem. Prod. Res. Develop*. **1973**, *12*, 294–301.

[16] Dwyer, F.G.; Catalysis for control of automotive emissions. *Catal. Rev.-Sci. Eng*. **1972**, *6*, 261–291.

[17] Graham, J.R.; Catalytic control of auto exhaust emissions, US Patent, 1973, 3741725.

[18] Meguerian, G.H.; Hirschberg, E.H.; Rakowsky, F.W.; Catalyst for treating exhaust gas from internal combustion engine, US Patent, 1977, 4006103.

[19] Hegedus, L.; Summers, J.C.; Platinum-rhodium for automotive emission control. US Patent, 1978, 4128506.

[20] Acres, G.J.K.; Cooper, B.J.; Automobile emission control systems-platinum catalysts for exhaust purification, *Platinum. Metals. Rev*. **1972**, *16*, 74–86.

[21] Hu, Z.; Allen, F.M.; Wan, C.Z.; Heck, R.M.; Steger, J.J.; Lakis, R.E.; Lyman, C.E.; Performance and structure of Pt-Rh three-way catalysts: mechanism for Pt/Rh synergism, *J. Catal*. **1998**, *174*, 13–21.

[22] Hu, Z.; A Pt-Rh synergism in Pt/Rh three-way catalysts, *Chem. Commun*. **1996**, 879–880.

[23] Matsuura, S.; Hirai, A.; Arimura, K.; Shinjoh, H.; Development of three-way catalyst with using only Pd as activator, SAE Paper 950257, 1995.

[24] Gandhi, H.S.; Graham, G.W.; McCabe, R.W.; Automotive exhaust catalysis, *J. Catal*. **2003**, *216*, 433–442.

[25] Chattha, M.S.; Watkins, W.L.H.; Gandhi, H.S.; Three-way catalyst for automotive emission control and method of making the catalyst, US Patent, 1991, 4992405.

[26] Shelef, M.; McCabe, R.W.; Twenty-five years after introduction of automotive catalysts: what next, *Catal. Today* **2000**, *62*, 35–50.

[27] Lui, Y.K.; Dettling, J.C.; Evolution of Pd/Rh TWC catalyst technology. SAE Paper 930249, 1993.

[28] Graham, G.W.; Potter, T.; Baird, R.J.; Gandhi, H.S.; Shelef, M.; Surface composition of polycrystalline Pd15Rh following high temperature oxidation in air, *J. Vacuum. Sci. Technol. A* **1986**, *4*, 1613–1616.

[29] Nunan, J.G.; Williamson, W.B.; Robota, H.J.; Henk, M.G.; Impact of Pt-Rh and Pd-Rh interactions on performance of bimetal catalysts, SAE Paper 950258, 1995.

[30] Summers, J.C.; Skowron, J.F.; Miller, M.J.; Use of light-off catalysts to meet the California LEV/ULEV standards, SAE Paper 930386, 1993.

[31] Lindner, D.; Lox, E.X.; van Yperen, R.; Ostgathe, K.; Reduction of exhaust gas emissions by using pd-based three-way catalysts, SAE Paper 960802, 1996.

[32] Cullis, C.F.; Willatt, B.M.; Oxidation of methane over supported precious metal catalysts, *J. Catal*. **1983**, *83*, 267–285.

[33] Yao, Y.F.Y; The oxidation of CO and hydrocarbons over noble metal catalysts, *J. Catal*. **1984**, *87*, 152–162.

[34] Gandhi, H.S.; Shelef, M.; Effects of sulphur on noble metal automotive catalysts, *Appl. Catal*. **1991**, *77*, 175–186.

[35] Gandhi, H.S.; Williamson, W.B.; Logothetis, E.M.; Tabock, J.; Peters, C.; Hurley, M.D.; Shelef, M.; Affinity of lead for noble metals on different supports, *Surf. Interface Anal*. **1984**, *6*, 149–161.

[36] Twigg, M.V.; Catalytic control of emissions from cars, *Catal. Today* **2011**, *163*, 33–41.

[37] Shelef, M.; Graham, G.W.; Why rhodium in automotive three-way catalysts, *Catal. Rev.-Sci. Eng*. **1994**, *36*, 433–457.

[38] Noh, J.; Yang, O.B.; Kim, D.H.; Woo, S.I.; Characteristics of the Pd-only three-way catalysts prepared by sol-gel method, *Catal. Today* **1999**, *53*, 575–582.

[39] Muraki, H.; Shinjoh, H.; Fujitani, Y.; Effect of lanthanum on the no reduction over palladium catalysts, *Appl. Catal*. **1986**, *22*, 325–335.

[40] Fernández-García, M.; Iglesias-Juez, A.; Martínez-Arias, A.; Hungría, A.B.; Anderson, J.A.; Conesa, J.C.; Soria, J.; Role of the state of the metal component on the light-off performance of Pd-based three-way catalysts, *J. Catal*. **2004**, *221*, 594–600.

[41] Iglesias-Juez, A.; Martínez-Arias, A.; Newton, M.A; Fiddy, S. G.; Fernández-García, M.; Redox behaviour of Pd-based TWCs under dynamic conditions: analysis using dispersive XAS and mass spectrometry, *Chem. Commun*. **2005**, 4092–4094.

[42] Lu, Y.; Kumar, M. S.; Chiarello, G. L.; Eggenschwiler, P. D.; Bach, C.; Weilenmann, M.; Spiteri, A.; Weidenkaff, A.; Ferri, D.; Operando XANES study of simulated transient cycles on a Pd-only three-way catalyst, *Catal. Commun*. **2013**, *39*, 55–59.

[43] Iglesias-Juez, A.; Kubacka, A.; Martínez-Arias, A.; Di Michiel, M.; Newton, M.A; Nanoparticulate Pd Supported Catalysts: Size-Dependent Formation of Pd(I)/Pd(0) and Their Role in CO Elimination, *J. Amer. Chem. Soc*. **2011**, *133*, 4484–4489.

[44] Brisley, R.J.; Chandler, G.R.; Jones, H.R.; Anderson, P.J.; Shady, P.J.; The use of palladium in advanced catalysts, SAE Paper 950259, 1995.

[45] Hu, Z.; Heck, R.M.; High temperature ultra-stable close-coupled catalysts. SAE Paper 1995, 950254.

[46] Kang, S.B.; Han, S. J.; Nam, S.B.; Nam, I.; Cho, B.K.; Kim, C.H.; Oh, S.H.; Activity function describing the effect of Pd loading on the catalytic performance of modern commercial TWC, *Chem. Eng. J*. **2012**, *207–208*, 117–121.

[47] Di Monte, R.; Fornasiero, P.; Kašpar, J.; Rumori, P.; Gubitosa, G.; Graziani, M.; $Pd/Ce_{0.6}Zr_{0.4}O_2/Al_2O_3$ as advanced materials for three-way catalysts Part 1. Catalyst characterisation, thermal stability and catalytic activity in the reduction of NO by CO, *Appl. Catal. B: Environ*. **2000**, *24*, 157–167.

[48] Mamede, A.S.; Leclercq, G.; Payen, E.; Grimblot, J.; Granger, P.; Surface Raman spectroscopic study of NO transformation over Pd-based catalysts, *Phys. Chem. Chem. Phys*. **2003**, *5*, 4402–4406.

[49] Daley, R.A.; Christou, S.Y.; Efstathiou, A.M.; Anderson, J.A.; Influence of oxychlorination treatments on the redox and oxygen storage and release properties of thermally aged $Pd\text{-}Rh/Ce_xZr_{1-x}O_2/Al_2O_3$ model three-way catalysts, *Appl. Catal. B: Environ*. **2005**, *60*, 117–127.

[50] Di Monte, R.; Fornasiero, P.; Kašpar, J.; Graziani, M.; Gatica, J.M.; Bernal, S.; Gómez-Herrero, A.; Stabilisation of nanostructured $Ce_{0.2}Zr_{0.8}O_2$ solid solution by impregnation on Al_2O_3: a suitable method for the production of thermally stable oxygen storage/release promoters for three-way catalysts, *Chem. Commun*. **2000**, 2167–2168.

[51] Shen, M.; Song, L.; Wang, J.; Wang, X.; Improved palladium only three-way catalysts using phosphorus modified alumina support, *Catal. Commun*. **2012**, *22*, 28–33.

[52] Ozawa, M.; Kimura, M.; Effect of cerium addition on the thermal stability of gamma alumina support, *J. Mater. Sci. Lett*. **1990**, *9*, 291–293.

[53] Shyu, J.Z.; Weber, W.H.; Gandhi, H.S.; Surface characterization of alumina-supported ceria, *J. Phys. Chem*. **1988**, *92*, 4964–4970.

[54] Piras, A.; Trovarelli, A.; Dolcetti, G.; Remarkable stabilization of transition alumina operated by ceria under reducing and redox conditions, *Appl. Catal. B: Environ*. **2000**, *28*, 77–81.

[55] Shyu, J.Z.; Otto, K.; Watkins, W.L.H.; Graham, G.W.; Belitz, R.K.; Ganhdi, H.S.; Characterization of Pd/γ-Alumina catalysts containing ceria, *J. Catal*. **1988**, *114*, 23–33.

[56] Burtin, P.; Brunelle, J.P.; Pijolat, M.; Soustelle, M.; Influence of surface area and additives on the thermal stability of transition alumina catalyst supports. I: Kinetic data, *Appl. Catal*. 1987, *34*, 225–238.

[57] Yamamoto, T.; Hatsui, T.; Matsuyama, T.; Tanaka, T.; Funabiki, T.; Structures and acid-base Properties of La/Al_2O_3-Role of La addition to enhance thermal stability of γ-Al_2O_3, *Chem. Mater*. **2003**, *15*, 4830–4840.

[58] Kwak, J. H.; Hu, J.; Lukaski, A.; Kim, D. H.; Szanyi, J.; Peden, C. H. F.; Role of pentacoordinated Al^{3+} ions in the high temperature phase transformation of γ-Al_2O_3, *J. Phys. Chem. C* **2008**, *112*, 9486–9492.

[59] Kašpar, J.; Fornasiero, P.; Graziani, M.; Use of CeO_2-based oxides in the three-way catalysis, *Catal. Today* **1999**, *50*, 285–298.

[60] Kim, G.; Ceria-promoted three-way catalysts for auto exhaust emission control, *Ind. Eng. Chem. Prod. Res. Dev*. **1982**, *21*, 267–274.

[61] Tagliaferri, S.; Köppel, R.A.; Baiker, A.; Influence of rhodium-and ceria-promotion of automotive palladium catalyst on its catalytic behaviour under steady-state and dynamic operation, *Appl. Catal. B: Environ*. **1998**, *15*, 159–177.

[62] Sanchez, M.G.; Gazquez, J.L.; Oxygen vacancy model in strong metal-support interaction, *J. Catal*. **1987**, *104*, 120–135.

[63] Holles, J.H.; Davis, R.J.; Murray, T.M.; Howe, J.M.; Effects of Pd particle size and ceria loading on NO reduction with CO, *J. Catal*. **2000**, *195*, 193–206.

[64] Ciuparu, D.; Bensalem, A.; Pfefferle, L.; Pd-Ce interactions and adsorption properties of palladium: CO and NO TPD studies over Pd-Ce/Al_2O_3 catalysts, *Appl. Catal. B: Environ*. **2000**, *26*, 241–255.

[65] Yao, H.C.; Yao, Y.F.Y.; Ceria in automotive exhaust catalysts, *J. Catal*. **1984**, *86*, 254–265.

[66] Zhao, M.W.; Shen, M.Q.; Wang, J.; Wang, W.L.; Influence of Pd morphology and support surface area on redox ability of Pd/$Ce_{0.67}Zr_{0.33}O_2$ under CO-He pulse and transient CO-O_2 measurements, *Ind. Eng. Chem. Res*. **2007**, *46*, 7883–7890.

[67] Yang, M.; Shen, M.; Wang, J. Wen, J.; Zhao, M; Wang, J.; Wang, W.; Pd-supported interaction-defined selective redox activities in Pd-$Ce_{0.7}Zr_{0.3}O_2$-Al_2O_3 model three-way catalysts, *J. Phys. Chem. C* **2009**, *113*, 12778–12789.

[68] Descorme, C.; Taha, R., Mouaddib-Moral, N.; Duprez, D.; Oxygen storage capacity measurements of three-way catalysts under transient conditions, *Appl. Catal*. A: Gen. **2002**, *223*, 287–299.

[69] Shelef, M.; Graham, G.W.; McCabe, R.W.; Ceria and other oxygen storage components in automotive catalysts, in: Trovarelli, A. (Ed.), *Catalysis by Ceria and Related Materials*; Imperial College Press, London, 2002, pp. 343–371.

[70] Tomohisa, O.; Kazuo, T.; Shinya, K.; Catalyst for purifying exhaust gas and method for production thereof, European Patent, 1989, 0337809 (A2).

[71] Martínez-Arias, A.; Fernández-García, M.; Hungría, A.B.; Iglesias-Juez, A.; Duncan, K.; Smith, R.; Anderson, J.A.; Conesa, J.C.; Soria, J.; Effect of thermal sintering on light-off performance of Pd/(Ce,Zr)Ox/Al_2O_3 three-way catalysts: model gas and engine tests, *J. Catal*. **2001**, *204*, 238–248.

[72] Cuif, J.P.; Blanchard, G.; Touret, O.; Seigneurin, A.; Marczi, M.; Quémeré, E.; (Ce, Zr)O_2 solid solutions for three-way catalysts, SAE Paper 970463, 1997.

[73] Fernández-García, M.; Martínez-Arias, A.; Hungría, A.B.; Iglesias-Juez, A.; Conesa, J.C.; Soria, J.; Thermal behavior of (Ce,Zr)Ox/Al_2O_3 complex oxides prepared by a microemulsion method. Phys. Chem. Chem. Phys. **2002**, *4*, 2473–2481.

[74] Ozawa, M.; Kimura, M.; Isogai, A.; The application of Ce-Zr oxide solid solution to oxygen storage promoters in automotive catalysts, *J. Alloy. Compd*. **1993**, *193*, 73–75.

[75] Granger, P.; Lamonier, J.F.; Sergent, N.; Aboukais, A.; Leclercq, L.; Leclercq, G.; Investigation of the intrinsic activity of $Zr_xCe_{1-x}O_2$ mixed oxides in the CO + NO reactions: influence of Pd incorporation, *Top. Catal*. **2001**, *16–17*, 89–94.

[76] Jen, H.W.; Graham, G.W.; Chun, W.; McCabe, R.W.; Cuif, J.P.; Deutsch, S.E.; Touret, O.; Characterization of model automotive exhaust catalysts: Pd on ceria and ceria-zirconia supports, *Catal. Today* **1999**, *50*, 309–328.

[77] Fornasiero, P.; Di Monte, R.; Rao, G.R.; Kašpar, J.; Meriani, S.; Trovarelli, A.; Graziani, M.; Rh-loaded CeO_2-ZrO_2 solid-solutions as highly efficient oxygen exchangers: dependence of the reduction Behavior and the oxygen storage capacity on the structural-properties, *J. Catal*. **1995**, *151*, 168–177.

[78] Balducci, G.; Kašpar, J.; Fornasiero, P.; Graziani, M.; Computer simulation studies of bulk reduction and oxygen migration in CeO_2-ZrO_2 solid solutions, *J. Phys. Chem. B* **1997**, *101*, 1750–1753.

[79] Balducci, G.; Kašpar, J.; Fornasiero, P.; Graziani, M.; Surface and reduction energetics of the CeO_2-ZrO_2 catalysts, *J. Phys. Chem. B* **1998**, *102*, 557–561.

[80] Graham, G.W.; Jen, H.W.; McCabe, R.W.; Straccia, A.W.; Haack, L.P.; Characterization of model automotive exhaust catalysts: Pd on Zr-rich ceria-zirconia supports, *Catal. Lett*. **2000**, *67*, 99–105.

[81] Fornasiero, P.; Balducci, G.; Di Monte, R.; Kašpar, J.; Sergo, V.; Gubitosa, G.; Ferrero,A.; Graziani, M.; Modification of the redox behaviour of CeO_2 induced by structural doping with ZrO_2, *J. Catal*. **1996**, *164*, 173–183.

[82] Fally, F.; Perrichon, V.; Vidal, H.; Kašpar, J.; Blanco, G.; Pintado, J.M.; Bernal, S.; Colon, G.; Daturi, M.; Lavalley, J.C.; Modification of the oxygen storage capacity of CeO_2-ZrO_2 mixed oxides after redox cycling aging, *Catal. Today* **2000**, *59*, 373–386.

[83] Vidal, H.; Kašpar, J.; Pijolat, M.; Colon, G.; Bernal, S.; Cordón, A.; Perrichon, V.; Fally, F.; Redox behavior of CeO_2-ZrO_2 mixed oxides I. Influence of redox treatments on high surface area catalysts, *Appl. Catal. B: Environ*. **2000**, *27*, 49–63.

[84] Fernandes, D.M.; Scofield, C.F.; Neto, A.A.; Cardoso, M.J.B.; Zotin, F.M.Z.; The influence of temperature on the deactivation of commercial Pd/Rh automotive catalysts, *Process Saf. Environ*. **2009**, *87*, 315–322.

[85] Martínez-Arias, A.; Fernández-García, M.; Iglesias-Juez, A.; Hungría, A.B.; Anderson, J.A.; Conesa, J.C.; Soria, J.; New Pd/$Ce_xZr_{1-x}O_2$/Al_2O_3 three-way catalysts prepared by microemulsion Part 2. In situ analysis of CO oxidation and

NO reduction under stoichiometric CO+NO+O_2, *Appl. Catal. B: Environ*. **2001**, *31*, 51–60.

[86] Fernández-García, M.; Martínez-Arias, A.; Iglesias-Juez, A.; Hungría, A.B.; Anderson, J.A.; Conesa, J.C.; Soria, J.; New $Pd/Ce_xZr_{1-x}O_2/Al_2O_3$ three-way catalysts prepared by microemulsion Part 1. Characterization and catalytic behavior for CO oxidation, *Appl. Catal. B: Environ*. **2001**, *31*, 39–50.

[87] Kubacka, A.; Iglesias-Juez, A.; Di Michiel, M.; Newton, M.A.; Fernández-García, M.; Influence of the Ce-Zr promoter on Pd behavior under dynamic CO/NO cycling conditions: a structural and chemical approach, *Phys. Chem. Chem. Phys*. **2013**, *15*, 8640–8647.

[88] Skoglundh, M.; Johansson, H.; Lijwendahl, L.; Jansson, K.; Dahl, L.; Hirschauer, B.; Cobalt-promoted palladium as a three-way catalyst, *Appl. Catal. B: Environ*. **1996**, *7*, 299–319.

[89] Logan, D.A.; Graham, G.W.; NO chemisorption on Pd (100) with ultra-thin overlayers of oxidized La and Al, *Surf. Sci. Lett*. **1992**, *277*, 47–51.

[90] Muraki, H.; Yokota, K.; Fujitani, Y.; Nitric oxide reduction performance of automotive palladium catalysts, *Appl. Catal*. **1989**, *48*, 93–105.

[91] Shinjoh, H.; Rare earth metals for automotive exhaust catalysts, *J. Alloy. Compd*. **2006**, 408–412, 1061–1064.

[92] Muraki, H.; Shinjoh, H.; Sobukawa, H.; Yokota, K.; Fujitani, Y.; Palladium-lanthanum catalysts for automotive emission control, *Ind. Eng. Chem. Prod. Res. Dev*. **1986**, *25*, 202–208.

[93] Adams, K.M.; Gandhi, H.S.; Palladium-tungsten catalysts for automotive exhaust treatment, *Ind. Eng. Chem. Prod. Res. Dev*. **1983**, *22*, 207–212.

[94] Halasz, I.; Brenner, A.; Catalytic reduction of nitric oxide on PdO-MoO_3/γ-Al_2O_3, *Appl. Catal. B: Environ*. **1993**, *2*, 131–146.

[95] Halasz, I.; Brenner, A.; Reduction of NO by CO on PdO-MoO_3/γ-Al_2O_3 of low molybdena loading, *Catal. Lett*. **1992**, *16*, 311–321.

[96] Schmal, M.; Baldanza, M.A.S.; Vannice, M.A.; Pd-xMo/Al_2O_3 catalysts for NO reduction by CO, *J. Catal*. **1999**, *185*, 138–151.

[97] Noronha, F.B.; Baldanza, M.A.S.; Schmal, M.; CO and NO adsorption on Alumina-Pd-Mo catalysts: effect of the precursor salts, *J. Catal*. **1999**, *188*, 270–280.

[98] Neyertz, C.; Volpe, M.; Preparation of binary palladium-vanadium supported catalysts from metal acetylacetonates, *Colloids Surf. A* **1998**, *136*, 63–69.

[99] Kim, D.H.; Woo, S.I.; Noh, J.; Yang, O.B.; Synergistic effect of vanadium and zirconium oxides in the Pd-only three-way catalysts synthesized by sol-gel method, *Appl. Catal. A: Gen*. **2001**, *207*, 69–77.

[100] Yentekakis, I.V.; Lambert, R.M.; Tikhov, M.S.; Konsolakis, M.; Kiousis, V.; Promotion by sodium in emission control catalysis: a kinetic and spectroscopic study of the Pd-catalyzed reduction of NO by propene, *J. Catal*. **1998**, *176*, 82–92.

[101] Macleod, N.; Isaac, J.; Lambert, R.M.; Sodium promotion of Pd/γ-Al_2O_3 catalysts operated under simulated "Three-Way" conditions. *J. Catal*. **2001**, *198*, 128–135.

[102] Sekiba, T.; Kimura, S.; Yamamoto, H.; Okada, A.; Development of automotive palladium three-way catalysts, *Catal. Today* **1994**, *22*, 113–126.

[103] Shinjoh, H.; Isomura, N.; Sobukawa, H.; Sugiura, M.; Effect of alkaline addition on hydrocarbon oxidation activities of palladium three-way catalyst, *Stud. Surf. Sci. Catal*. **1998**, *116*, 83–91.

[104] Kobayashi, T.; Yamada, T.; Kayano, K.; Effect of basic metal additives on NO*x* reduction property of Pd-based three-way catalyst, *Appl. Catal. B: Environ*. **2001**, *30*, 287–292.

[105] Mikulova, J.; Rossignol, S.; Gérard, F.; Mesnard, D.; Kappenstein, C.; Duprez, D.; Properties of cerium-zirconium mixed oxides partially substituted by neodymium: Comparison with Zr-Ce-Pr-O ternary oxides, *J. Solid State Chem*. **2006**, *179*, 2511–2520.

[106] Guo, J.X.; Wu, D.D.; Zhang, L.; Gong, M.C.; Zhao, M.; Chen, Y.Q.; Preparation of nanometric CeO_2-ZrO_2-Nd_2O_3 solid solution and its catalytic performances, *J. Alloy. Compd*. **2008**, *460*, 485–490.

[107] Wu, X.D.; Wu, X.D.; Liang, Q.; Fan, J.; Weng, D.; Xie, Z.; Wei, S.Q.; Structure and oxygen storage capacity of Pr/Nd doped CeO_2-ZrO_2 mixed oxides, *Solid State Sci*. **2007**, *9*, 636–643.

[108] Wang, W.D.; Lin, P.Y.; Meng, M.; Fu, Y.L.; Hu, T.D.; Xie, Y.N.; Liu, T.; Promoter of (Ce-Zr)O_2 solid solution modified by praseodymia in three-way catalysts, *J. Rare Earth* **2003**, *21*, 430–435.

[109] Wang, Q.Y.; Li, G.F.; Zhao, B.; Zhou, R.X.; Investigation on properties of a novel ceria-zirconia -praseodymia solid solution and its application in Pd-only three-way catalyst for gasoline engine emission control, *Fuel* **2011**, *90*, 3047–3055.

[110] Wang, Q.Y.; Li, G.F.; Zhao, B.; Zhou, R.X.; The effect of Nd on the properties of ceria-zirconia solid solution and the catalytic performance of its supported Pd-only three-way catalyst for gasoline engine exhaust reduction, *J. Hazard. Mater*. **2011**, *189*, 150–157.

[111] Wang, Q.Y.; Li, G.F.; Zhao, B.; Zhou, R.X.; The effect of rare earth modification on ceria-zirconia solid solution and its application in Pd-only three-way catalyst, *J. Mol. Catal. A: Chem*. **2011**, *339*, 52–60.

[112] Vidmar, P.; Fornasiero, P.; Kašpar, J.; Gubitosa, G.; Graziani, M.; Effects of trivalent dopants on the redox properties of $Ce_{0.6}Zr_{0.4}O_2$ mixed oxide, *J. Catal*. **1997**, *171*, 160–168.

[113] Markaryan, G.L.; Ikryannikova, L.N.; Muravieva, G.P.; Turakulova, A.O.; Kostyuk, B.G.; Lunina, E.V.; Lunin, V.V.; Zhilinskaya, E.; Aboukais, A.; Redox properties and phase composition of CeO_2-ZrO_2 and Y_2O_3-CeO_2-ZrO_2 solid solutions, *Colloids Surf. A* **1999**, *151*, 435–447.

[114] Hu, Y.C.; Hydrothermal synthesis of nano Ce-Zr-Y oxide solid solution for automotive three-way catalyst, *J. Amer. Ceram. Soc*. **2006**, *89*, 2949–2951.

[115] Yamamoto, M.; Tanaka, H.; Influence of support materials on durability of palladium in three-way catalyst, SAE Paper 980664, 1998.

[116] Yamada, K.; Tanaka, H.; Yamamoto, M.; Oxygen storage capacity on cerium oxide-precious metal system, SAE Paper 970464, 1997.

[117] Wang, G.; Meng, M.; Zha, Y.; Ding, T.; High-temperature close coupled catalysts Pd/Ce-Zr-M/Al_2O_3 (M = Y, Ca or Ba) used for the total oxidation of propane, *Fuel* **2010**, *89*, 2244–2251.

[118] Wang, G., You,R., Meng, M., An optimized highly active and thermo-stable oxidation catalyst Pd/Ce-Zr-Y/Al_2O_3 calcined at super high temperature and used for C_3H_8 total oxidation, *Fuel* **2013**, *103*, 799–804.

[119] Li, G.F.; Wang, Q.Y.; Zhao, B.; Shen, M.Q.; Zhou, R.X.; Effect of iron doping into CeO_2-ZrO_2 on the properties and catalytic behaviour of Pd-only three-way catalyst for automotive emission control, *J. Hazard. Mater*. **2011**, *186*, 911–920.

[120] Li, G.F.; Zhao, B.; Wang, Q.Y.; Zhou, R.X.; The effect of Ni on the structure and catalytic behavior of model $Pd/Ce_{0.67}Zr_{0.33}O_2$ three-way catalyst before and after aging, *Appl. Catal. B: Environ*. **2010**, *97*, 41–48.

[121] Li, G.F.; Wang, Q.Y.; Zhao, B.; Zhou, R.X.; A new insight into the role of transition metals doping with CeO_2-ZrO_2 and its application in Pd-only three-way catalysts for automotive emission control, *Fuel* **2012**, *92*, 360–368.

[122] Guo, Y.; Lu, G.; Zhang, Z.; Zhang, S.; Qi,Y.; Liu, Y.; Preparation of $Ce_xZr_{1-x}O_2$ ($x = 0.75, 0.62$) solid solution and its application in Pd-only three-way catalysts. *Catal. Today* **2007**, *126*, 296–302.

[123] Yao, Y. Fang, R. Shi, Z.; Gong M.; Chen Y.; The Effect of La_2O_3 on Pd Close-Coupled Catalysts. Chin, *J. Catal*. **2011**, *32*, 589–594.

[124] Hungría, A.B.; Browning, N.D.; Erni, R.P.; Fernández-García, M.; Conesa, J.C.; Pérez-Omil, J.A. Martínez-Arias, A.; The effect of Ni in Pd-Ni/(Ce,Zr)Ox/Al_2O_3 catalysts used for stoichiometric CO and NO elimination. Part 1: Nanoscopic characterization of the catalysts, *J. Catal*. **2005**, *235*, 251–261.

[125] Hungría, A.B.; Fernández-García, M.; Anderson, J.A.; Martínez-Arias, A.; The effect of Ni in Pd-Ni/(Ce,Zr)O*x*/Al_2O_3 catalysts used for stoichiometric CO and NO elimination. Part 2: Catalytic activity and in situ spectroscopic studies, *J. Catal*. **2005**, *235*, 262–271.

[126] Hungría, A.B.; Iglesias-Juez, A.; Martínez-Arias, A.; Fernández-García, M.; Anderson, J.A.; Conesa, J.C.; Soria, J.; Effects of copper on the catalytic properties of bimetallic Pd-Cu/(Ce,Zr)O*x*/Al_2O_3 and Pd-Cu/(Ce,Zr)O*x* catalysts for CO and NO elimination, *J. Catal*. **2002**, *206*, 281–294.

[127] Illas, F.; López, N.; Ricart, J. M.; Clotet, A.; Conesa, J.C.; Fernández-García, M.; Interaction of CO and NO with PdCu(111) surfaces, *J. Phys. Chem. B* **1998**, *102*, 8017–8023.

[128] Iglesias-Juez, A.; Hungría, A.B.; Martínez-Arias, A.; Anderson, J.A.; Fernández-García, M.; Pd-based (Ce,Zr)O*x*-supported catalysts: Promoting effect of base metals (Cr, Cu, Ni) in CO and NO elimination, *Catal. Today* **2009**, *143*, 195–202.

[129] Hadi, A.; Yaacob, I.I.; Synthesis of PdO/CeO_2 mixed oxides catalyst for automotive exhaust emissions control, *Catal. Today* **2004**, *96*, 165–170.

[130] Zhou, K.B.; Chen, H.D.; Tian, Q.; Hao, Z.P.; Shen, D.X.; Xu, X.B.; Pd-containing perovskite-type oxides used for three-way catalysts, *J. Mol. Catal. A: Chem*. **2002**, *189*, 225–232.

[131] Nishihata, Y.; Mizuki, J.; Akao, T.; Tanaka, H.; Uenishi, M.; Kimura, M.; Okamoto, T.; Hamadak, N.; Self-regeneration of a Pd-perovskite catalyst for automotive emissions control, *Nature* **2002**, *418*, 164–167.

[132] Masuda, K.; Sano, T.; Mizukami, F.; Kuno, K.; preparation on the thermostability and the oxidation activity of CeO*x*/BaO/Al_2O_3-supported Pd catalysts, *Appl. Catal. A: Gen*. **1995**, *133*, 59–65.

[133] Uenishi, M.; Taniguchi, M.; Tanaka, H.; Kimura, M.; Nishihata, Y.; Mizuki, J.; Kobayashi, T.; Redox behavior of palladium at start-up in the perovskite-type LaFePdO*x* automotive catalysts showing a self-regenerative function, *Appl. Catal. B: Environ*. **2005**, *57*, 267–273.

[134] Bera, P.; Patil, K.C.; Jayaram, V.; Subbanna, G.N.; Hegde, M.S.; Ionic Dispersion of Pt and Pd on CeO_2 by Combustion Method: Effect of metal-ceria interaction on catalytic activities for NO reduction and CO and hydrocarbon oxidation, *J. Catal*. **2000**, *196*, 293–301.

[135] Roy, S.; Hegde, M.S.; Pd ion substituted CeO_2: A superior de-NO*x* catalyst to Pt or Rh metal ion doped ceria, *Catal. Commun*. **2008**, *9*, 811–815.

[136] Kim, D.H.; Woo, S.I.; Yang, O.B.; Effect of pH in a sol-gel synthesis on the physicochemical properties of Pd-alumina three-way catalyst, *Appl. Catal. B: Environ*. **2000**, *26*, 285–289.

[137] Monteiro, R.S.; Dieguez, L.C.; Schmal, M.; The role of Pd precursors in the oxidation of carbon monoxide over Pd/Al_2O_3 and $Pd/CeO_2/Al_2O_3$ catalysts, *Catal. Today* **2001**, *65*, 77–89.

[138] Zhu, Z.; Lu, G.; Guo, Y.; Guo, Y.; Zhang, Z.; Wang, Y.; Influences of Pd precursors and preparation method on the catalytic performances of Pd-only close-coupled catalysts, *J. Ind. Eng. Chem*. **2012**, *18*, 2135–2140.

[139] van den Tillaart, J.A.A.; Leyrer, J.; Eckhoff, S.; Lox, E.S.; Effect of support oxide and noble metal precursor on the activity of automotive diesel catalysts, *Appl. Catal. B: Environ*. **1996**, *10*, 53–68.

[140] Kim, D.H.; Woo, S.I.; Lee, J.M.; Yang, O.B.; The role of lanthanum oxide on Pd-only three-way catalysts prepared by co-impregnation and sequential impregnation methods, *Catal. Lett*. **2000**, *70*, 35–41.

[141] Garcia, T.; Weng, W.H.; Solsona, B.J.; Carter, E.; Carley A.F.; Kiely, C.J.; Taylor, S.H.; The significance of the order of impregnation on the activity of vanadia promoted palladium-alumina catalysts for propane total oxidation, *Catal. Sci. Technol*. **2011**, *1*, 1367–1375.

[142] Wang, Q.Y.; Li, Z.G.; Zhao, B.; Li, G.F.; Zhou, R.X.; Effect of synthesis method on the properties of ceria-zirconia modified alumina and the catalytic performance of its supported Pd-only three-way catalyst, *J. Mol. Catal. A: Chem*. **2011**, *344*, 132–137.

[143] Suna, Y.H.; Sermon, P.A.; Surface reactivity and bulk properties of ZrO_2, Part 2–Importance of homogeneity in the stabilisation of high surface area CeO_2-ZrO_2 aerogels, *J. Mater. Chem*. **1996**, *6*, 1025–1029.

[144] Terribile, D.; A. Trovarelli, Llorca, J.; de Leitenburg, C.; Dolcetti, G.; The preparation of high surface area CeO_2-ZrO_2 mixed oxides by a surfactant-assisted approach, *Catal. Today* **1998**, *43*, 79–88.

[145] Chen, L.F.; González, G.G.; Wang, J.A.; Noreña, L.E.; Toledo, A.; Castillo, S.; Morán-Pineda, M.; Surfactant-controlled synthesis of $Pd/Ce_{0.6}Zr_{0.4}O_2$ catalyst for NO reduction by CO with excess oxygen, *Appl. Surf. Sci*. **2005**, *243*, 319–328.

[146] Luo, M.F.; Zheng, X.M.; Redox behaviour and catalytic properties of $Ce_{0.5}Zr_{0.5}O_2$-supported palladium catalysts, *Appl. Catal*. A: Gen. **1999**, *189*, 15–21.

[147] Chen, H.R.; Ye, Z.Q.; Cui, X.Z.; Shi, J.L.; Yan, D.S.; A novel mesostructured alumina-ceria-zirconia tri-component nanocomposite with high thermal stability and its three-way catalysis, *Micropor. Mesopor. Mat*. **2011**, *143*, 368–374.

[148] Trovarelli, A.; Zamar, F.; Llorca, J.; Leitenburg, C.; Dolcetti, G.; Kissz, J.T.; Nanophase fluorite- structured CeO_2-ZrO_2 catalysts prepared by high-energy mechanical milling, *J. Catal*. **1997**, *169*, 490–502.

[149] Gallopoulos, N.E.; Bridging the present to the future in personal transportation-the role of internal combustion engines, SAE Paper 920721, 1992.

[150] Laing, P.M.; Development of an alternator-powered electrically-heated catalyst system, SAE Paper 941042, 1994.

[151] Kim, D.J.; Kim, J.W.; Yie, J.E.; Temperature-programmed adsorption and characteristics of honeycomb hydrocarbon adsorbers, *Ind. Eng. Chem. Res*. **2002**, *41*, 6589–6592.

[152] Chen, S.F.; Amundsen, A.R.; Rabinowitz, H.N.; Yamada, T.; The development of a close coupled plus underfloor catalyst for a ULEV application, SAE Paper 960796, 1996.

[153] Matsumoto, S.; Recent advances in automobile exhaust catalyst, *Catal. Surv. Jpn*. **1997**, *1*, 111–117

[154] Härkönen, M.; Kivioja, M.; Lappi, P.; Mannila, P.; Maunula, T.; Slotte, T.; Performance and durability of palladium only metallic three-way catalyst, SAE Paper 940935, 1994.

[155] Beck, D.D.; Sommers, J.W.; Impact of sulfur on the performance of vehicle-aged palladium monoliths. *Appl. Catal. B: Environ*. **1995**, *6*, 185–200.

[156] Heck, R.M.; Hu, Z.; Smaling, R.; Amundsen, A.; Close coupled catalyst system design and ULEV performance after 1050°C aging, SAE Paper 952415, 1995.

[157] Hu, Z.; Heck, R.M.; Rabinowitz, H.N.; Close-coupled catalyst, US Patent, 2000, 6044644.

[158] Hu, Z.; Heck, R.M.; Rabinowitz, H.N.; Method for using a close-coupled catalyst, US Patent, 2001, 6254842B1.

[159] Williamson, W.B.; Richmond, R.P.; Nunan, J.G.; Bortun, A.; Robota, H.J.; Palladium and platinum/rhodium dual-catalyst NLEV and tier II a close-coupled emission solutions. SAE Paper 2001-01-0923, 2001.

[160] Williamson, W.B.; Dou, D.; Robota, H.J.; Dual-catalyst undefloor LEV/ULEV strategies for effective precious metal management, SAE Paper 1999-01-0776, 1999.

[161] Bernal, S.; Calvino, J.J.; Cauqui, M.A.; Gatica, J.M.; Larese, C.; Pérez Omil, J.A.; Pintado, J.M.; Some recent results on metal/support interaction effects in NM/CeO_2 (NM: noble metal) catalysts, *Catal. Today* **1999**, *50*, 175–206.

[162] Hu, Z.; Wan, C.Z.; Lui, Y.K.; Dettling, J.; Layered catalyst composite, US Patent, 1997, 5597771.

[163] Hu, Z.; Wan, C.Z.; Lui, Y.K.; Dettling, J.; Steger, J.J.; Design of a novel Pd three-way catalyst: integration of catalytic functions in three dimensions, *Catal. Today* **1996**, *30*, 83–89.

[164] Aoki, Y.; Sakagami, S.; Kawai, M.; Takahashi, N.; Tanabe, T.; Sunada, T.; Development of advanced zone-coated three-way catalysts, SAE Paper 2011-01-0296, 2011.

[165] Taylor, K.C. Nitric oxide catalysis in automotive exhaust systems, *Catal. Rev.-Sci. Eng*. **1993**, *35*, 457–481.

[166] Muraki, H.; Shinjoh, H.; Fujitani, Y.; Reduction of NO by CO over alumina-supported palladium catalyst, *Ind. Eng. Chem. Prod. Res. Dev*. **1986**, *25*, 419–424.

[167] Holles, J.H.; Switzer, M.A.; Davis, R.J.; Influence of ceria and lanthana promoters on the kinetics of NO and N_2O reduction by CO over alumina-supported palladium and rhodium, *J. Catal*. **2000**, *190*, 247–260.

[168] Mamede, A.S.; Leclercq, G.; Payen, E.; Granger, P.; Grimblot, J.; In situ Raman characterisation of surface modifications during NO transformation over automotive Pd-based exhaust catalysts, *J. Mol. Struct*. **2003**, *651–653*, 353–364.

[169] Hamdaoui, A.E.; Bergeret, G.; Massardier, J.; Primet, M.; Renouprez, A.; CO and NO interaction with Pd-Ag and Pd-Cr bimetallic catalysts, *J. Catal*. **1994**, *148*, 47–55.

[170] Granger, P.; Dhainaut, F.; Pietrz, S.; Malfoy, P.; Mamede, A.S.; Leclercq, L.; Leclercq, G.; An overview: Comparative kinetic behaviour of Pt, Rh and Pd in the NO + CO and NO + H_2 reactions, *Top. Catal*. **2006**, *39*, 65–76.

[171] Rainer, D.R.; Koranne, M.; Vesecky, S.M.; Goodman, D.W.; CO + O_2 and CO + NO reactions over Pd/Al_2O_3 catalysts, *J. Phys. Chem. B* **1997**, *101*, 10769–10774.

[172] Rainer, D.R.; Vesecky, S.M.; Koranne, M.; Koranne, M.; Oh, W.S.; Goodman, D.W.; The CO+NO reaction over Pd: a combined study using single-crystal, planar-model-supported, and high-surface-area Pd/Al_2O_3 catalysts, *J. Catal*. **1997**, *167*, 234–241.

[173] Almusaiteer, K.; Chuang, S.S.C.; Isolation of active adsorbates for the NO-CO reaction on Pd/Al_2O_3 by selective enhancement and selective poisoning, *J. Catal*. **1998**, *180*, 161–170.

[174] Almusaiteer, K.; Chuang, S.S.C.; Dynamic behavior of adsorbed NO and CO under transient conditions on Pd/Al_2O_3, *J. Catal*. **1999**, *184*, 189–201.

[175] Sica, A.M.; Gigola, C.E.; Interaction of CO, NO and NO/CO over Pd/γ-Al_2O_3 and Pd-WOx/γ-Al_2O_3 catalysts, *Appl. Catal. A: Gen*. **2003**, *239*, 121–139.

[176] Newton, M.A.; Di Michiel, M.; Kubacka, A.; Fernández-García, M.; Combining time-resolved hard x-ray diffraction and diffuse reflectance infrared spectroscopy to illuminate CO dissociation and transient carbon storage by supported Pd nanoparticles during CO/NO cycling, *J. Amer. Chem. Soc*. **2010**, *132*, 4540–4541.

[177] Matam, S. K.; Newton, M. A.; Weidenkaff, A.; Ferri, D.; Time resolved operando spectroscopic study of the origin of phosphorus induced chemical aging of model three-way catalysts Pd/Al_2O_3, *Catal. Today* **2013**, *205*, 3–9.

[178] Graham, G.W.; Logan, A.D.; Shelef, M.; Oxidation of CO by O_2, NO, and mixtures of O_2 and NO over Pd (100), *J. Phys. Chem*. **1993**, *97*, 5445–5446.

[179] Kubacka, A.; Martínez-Arias, A.; Fernández-García, M.; Di Michiel, M.; Newton, M. A.; Multitechnique analysis of supported Pd particles upon dynamic, cycling CO/NO conditions: Size-dependence of the structure–activity relationship, *J. Catal*. **2010**, *270*, 275–284.

[180] Newton, M. A.; Di Michiel, M.; Kubacka, A.; Iglesias-Juez, A.; Fernández-García, M.; Observing oxygen storage and release at work during cycling redox conditions: synergies between noble metal and oxide promoter, *Angew. Chem. Int. Ed*. **2012**, *51*, 2363–2367.

[181] Macleod, N.; Lambert, R.M.; An in situ DRIFTS study of efficient lean NOx reduction with H_2 + CO over Pd/Al_2O_3: the key role of transient NCO formation in the subsequent generation of ammonia, *Appl. Catal. B: Environ.* **2003**, *46*, 483–495.

[182] Kobylinski, T.P.; Taylor, B.W.; The catalytic chemistry of nitric oxide: II. Reduction of nitric oxide over noble metal catalysts, *J. Catal*. **1974**, *33*, 376–384.

[183] Dhainaut, F.; Pietrzyk, S.; Granger, P.; Kinetics of the NO + H_2 reaction over supported noble metal based catalysts: Support effect on their adsorption properties, *Appl. Catal. B: Environ*. **2007**, *70*, 100–110.

[184] Dhainaut, F.; Pietrzyk, S.; Granger, P.; Kinetic investigation of the NO reduction by H_2 over noble metal based catalysts, *Catal. Today* **2007**, *119*, 94–99.

[185] Paredis, K.; Ono, L. K.; Behafarid, F.; Zhang, Z.; Yang, J.C.; Frenkel, A.I.; Cuenya, B.R.; Evolution of the structure and chemical state of Pd nanoparticles during the in situ catalytic reduction of NO with H_2, *J. Amer. Chem. Soc*. **2011**, *133*, 13455–13464.

[186] Chambers, D.C.; Angove, D.E.; Cant, N.W.; The formation and hydrolysis of isocyanic acid during the reaction of NO, CO, and H_2 mixtures on supported platinum, palladium, and rhodium, *J. Catal*. **2001**, *204*, 11–22.

[187] Rahkamaa-Tolonen, K.; Salmi,T.; Murzin, D.Y.; Dillon, L.B.; Lassi, U.; Keiski, R. L.; Investigation of NO reduction by H_2 on Pd monolith with transient and isotopic exchange techniques II. H_2/D_2 exchange in the reduction of NO, *J. Catal*. **2002**, *210*, 30–38.

[188] Oh, S. H.; Triplett, T.; Reaction pathways and mechanism for ammonia formation and removal over palladium-based three-way catalysts: Multiple roles of CO, *Catal. Today* **2014**, *231*, 22–32.

[189] Schwab, G. M.; Gossner, K.; The carbon monoxide combustion via silver, palladium and their alloy, *Z. Phys. Chem*. **1958**, *16*, 39–63 (in German).

[190] Engel, T.; Ertl, G.; A molecular beam investigation of the catalytic oxidation of CO on Pd (111), *J. Chem. Phys*. **1978**, *69*, 1267–1281.

[191] Szanyi, J.; Kuhn, K.; Goodman, D.W.; CO oxidation on palladium. 2. A combined kinetic-infrared reflection absorption spectroscopic study of Pd (111), *J. Phys. Chem*. **1994**, *98*, 2978–2981.

[192] Xu, X.; Goodman, D.W.; An infrared and kinetic study of CO oxidation on model silica-supported palladium catalysts from 10^{-9} to 15 Torr, *J. Phys. Chem*. **1993**, *97*, 7711–7718.

[193] Balmes, O.; Resta, A.; Wermeille,D.; Felici, R.; Messing, M. E.; Deppert, K. Liu, Z.; Grass, M. E.; Bluhm, H.; van Rijn, R.; Frenken, J.W. M.; Westerström, R.; Blomberg, S.; Gustafson, J.; Andersen, J. N.; Lundgreng, E.; Reversible formation of a PdC*x* phase in Pd nanoparticles upon CO and O_2 exposure, *Phys. Chem. Chem. Phys*. **2012**, *14*, 4796–4801.

[194] Parker, S. F.; The role of hydroxyl groups in low temperature carbon monoxide oxidation, *Chem. Commun*. **2011**, *47*, 1988–1990.

[195] Föttinger, K.; Schlögl, R.; Rupprechter, G.; The mechanism of carbonate formation on Pd-Al_2O_3 catalysts, *Chem. Commun*. **2008**, 320–322.

[196] Rajasree, R.; Hoebink, J.H.B.J.; Schouten, J.C.; Transient kinetics of carbon monoxide oxidation by oxygen over supported palladium/ceria/zirconia three-way catalysts in the absence and presence of water and carbon dioxide, *J. Catal*. **2004**, *223*, 36–43.

[197] Kotareva, I.A.; Oshanina, I.V.; Odintsov, K.Y.; Bruk, L.G.; Temkin, O.N.; Kinetics and mechanism of carbon monoxide oxidation on the supported metal complex catalyst $PdCl_2$-$CuCl_2/Al_2O_3$, *Kinet. Catal*. **2008**, *49*, 22–30.

[198] Petrova, M.V.; Williams, F.A.; A small detailed chemical-kinetic mechanism for hydrocarbon combustion, *Combust. Flame* **2006**, *144*, 526–544.

[199] Ma, L.; Bart, H.; Ning, P.; Zhang, A.; Wu, G.; Zhu, Z.; Kinetic study of three-way catalyst of automotive exhaust gas: Modeling and application, *Chem. Eng. J*. **2009**, *155*, 241–247.

[200] van de Beld, L.; van der Ven, M.C.; Westerterp, K.R.; A kinetic study of the complete oxidation of ethene, propane and their mixtures on a Pd/Al_2O_3 catalyst, *Chem. Eng. Proc*. **1995**, *34*, 469–478.

[201] Cullis, C. F.; Nevell, T. G.; The kinetics of the catalytic oxidation over palladium of some alkanes and cycloalkanes, *Proc. R. Soc. Lond. A* **1976**, *349*, 523–534.

[202] Yao, Y.F.Y.; Oxidation of alkanes over noble metal catalysts, *Ind. Eng. Chem. Prod. Res. Dev*. **1980**, *19*, 293–298.

[203] Aryafar, M.; Zaera, F.; Kinetic study of the catalytic oxidation of alkanes over nickel, palladium, and platinum foils, *Catal. Lett*. **1997**, *48*, 173–183.

[204] Iglesias-Juez, A.; Martínez-Arias, A.; Fernández-García, M.; Metal-promoter interface in $Pd/(Ce,Zr)Ox/Al_2O_3$ catalysts: effect of thermal aging, *J. Catal*. **2004**, *221*, 148–161.

[205] Xu, Q.; Kharas, K.C.; Croley, B.J.; Datye, A.K.; The sintering of supported Pd automotive catalysts, *Chem. Cat, Chem*. **2011**, *3*, 1004–1014."

[206] Birgersson, H.; Boutonnet, M.; Klingstedt, F.; Murzin, D.Y.; Stefanov, P.; Naydenov, A.; An investigation of a new regeneration method of commercial aged three-way catalysts, *Appl. Catal. B: Environ*. **2006**, *65*, 93–100.

[207] Williamson, W.B.; Lewis, D.; Perry, J.; Gandhi, H.S.; Durability of Palladium Automotive Catalysts: Effects of trace lead levels, exhaust composition, and misfueling, *Ind. Eng. Chem. Prod. Res. Dev*. **1984**, *23*, 531–536.

[208] Hansen,T. W.; Delariva, A. T.; Challa,S. R.; Datye, A. K.; Sintering of catalytic nanoparticles: particle migration or ostwald ripening?, *Acc. Chem. Res*. **2013**, *46*, 1720–1730.

[209] Wynblatt,P.; Gjostein,N.; A. Supported metal crystallites, *Prog. Solid State Chem*. **1975**, *9*, 21–58.

[210] McCarty, J. G.; Malukhin, G.; Poojary, D. M.; Datye, A. K.; Xu, Q.; Thermal coarsening of supported palladium combustion catalysts, *J. Phys. Chem. B* **2005**, *109*, 2387–2391.

[211] Kang, S.B.; Kwon, H.J.; Nam, I.S.; Activity function for describing alteration of three-way catalyst performance over palladium-only three-way catalysts by catalyst mileage, *Ind. Eng. Chem. Res*. **2011**, *50*, 5499–5509.

[212] Datye, A.K.; Bravo, J.; Nelson, T.R.; Atanasova, P.; Lyubovsky, M.; Pfefferle, L.; Catalyst microstructure and methane oxidation reactivity during the Pd-PdO transformation on alumina supports, *Appl. Catal. A: Gen*. **2000**, *198*, 179–196.

[213] Kang, S. B.; Han, S. J.; Nam, S. B.; Nam, I.S.; Cho, B. K.; Kim, C. H.; Oh, S. H.; Effect of Aging Atmosphere on Thermal Sintering of Modern Commercial TWCs, *Top. Catal*. **2013**, *56*, 298–305.

[214] Martínez-Arias, A.; Fernández-García, M.; Iglesias-Juez, A.; Hungría, A.B.; Anderson, J.A.; Conesa, J.C.; Soria, J.; Influence of thermal sintering on the activity for $CO\text{-}O_2$ and $CO\text{-}O_2$-NO stoichiometric reactions over $Pd/(Ce, Zr)Ox/Al_2O_3$ catalysts, *Appl. Catal. B: Environ*. **2002**, *38*, 151–158.

[215] Heo, I.; Choung, J.W.; Kim, P.-S.; Nam, I.S.; Song, Y.L.; In, C.B.; Yeo, G.K.; The alteration of the performance of field-aged Pd-based TWCs towards CO and C_3H_6 oxidation, *Appl. Catal. B: Environ*. **2009**, *92*, 114–125.

[216] Xu, L.; Guo, G.; Dairene, U.; O'Neill, A.E.; Weber, W.H.; Rokosz, M.J.; McCabe, R.W.; Cerium phosphate in automotive exhaust catalyst poisoning, *Appl. Catal. B: Environ*. **2004**, *50*, 113–125.

[217] O'Neill, A.E.; Dairene, U.; Raman studies of automotive catalyst deactivation, SAE Paper 2006–01-0409, 2006.

[218] Christou, S.Y.; García-Rodríguez, S.; Fierro, J.L.G.; Efstathiou, A.M.; Deactivation of $Pd/Ce_{0.5}Zr_{0.5}O_2$ model three-way catalyst by P, Ca and Zn deposition, *Appl. Catal. B: Environ*. **2012**, *111–112*, 233–245.

[219] Hilaire, S.; Sharma, S.; Gorte, R.J.; Vohs, J.M.; Jen, H.W.; Effect of SO_2 on the oxygen storage capacity of ceria-based catalysts, *Catal. Lett*. **2000**, *70*, 131–135.

[220] Boaro, M.; de Leitenburg, C.; Dolcetti, G.; Trovarelli, A.; Graziani, M.; Oxygen storage behavior of ceria-zirconia-based catalysts in the presence of SO_2, *Top. Catal*. **2001**, *16–17*, 299–306.